Journal of Engineering Research

Volume 9
Issue 1 *issue 1*

Article 19

# Numerical Analysis of Cold-Formed Built-Up Battened Steel Columns Under Eccentric Compressive Loading

mai mohamed sheta
*Department of construction and building Engineering, Higher Institute for Engineering, 6th of October City, Egypt*, maisheta39@gmail.com

Hanan Hussein Eltobgy
*Department of Civil Engineering, Faculty of Engineering at Shoubra, Benha University, Egypt*, hanan.altobgy@feng.bu.edu.eg

Mohamed Massoud El Saadawy
*Housing and Building National Research Center (HBRC),87El Tahrir St., Dokki, Giza11511, POBox1770, Cairo, Egypt*, m_massoud2002@yahoo.com

Khaled abdallah Gharib
*Department of Civil Engineering, Faculty of Engineering at Shoubra, Benha University, Egypt*, khaled.Gharib@feng.bu.edu.eg

Journal of Engineering Research (JER)
ISSN: 2356-9441 Vol. 9 – No. 1, 2025 ©Tanta University, Faculty of Engineering e ISSN: 2735-4873

# Numerical Analysis of Cold-Formed Built-Up Battened Steel Columns Under Eccentric Compressive Loading

Mai M.Sheta[1*], Hanan H. Eltobgy[2], Mohamed M. El-Saadawy[3], and Khaled A. M. Gharib[4]
[1] Department of construction and building Engineering, Higher Institute for Engineering, 6th of October City, Egypt
[2]Department of Civil Engineering, Faculty of Engineering at Shoubra, Benha University, Egypt
[3]Housing and Building National Research Center (HBRC),87El Tahrir St., Dokki, Giza11511, POBox1770, Cairo, Egypt
[4]Department of Civil Engineering, Faculty of Engineering at Shoubra, Benha University, Egypt
*Corresponding author's email: maisheta39@gmail.com

***Abstract*- This paper presents a 3D finite element model simulation using ABAQUS finite element software to investigate the behavior of steel battened beam columns under uniaxial loads. The columns consist of double-channel cold-formed slender open sections. The study highlighted the effects of various factors on the ultimate capacity of these beam-column members.**

**By considering both global and local imperfections, the model focuses on the structural strength and performance of battened cold-formed steel columns made from built-up sections. These cold-formed steel (CFS) columns have a slenderness ratio ranging from 50 to 162. Axial loads are applied at the pin-ended support of the column, which comprises two cold-formed steel open-channel sections positioned at varying center-to-center distances.**

**To validate the finite element models, their results were compared with relevant experimental data from the literature on similar geometries. The finite element analysis accounted for various factors, including different geometrical properties of column sections, slenderness ratios, nonlinear material properties of cold-formed steel sections, built-up section components, and initial geometric imperfections.**

**Finally, the analysis results were compared to the predicted ultimate strengths according to both the North American Specification and European codes EC3. The findings show that the strength of battened columns is strongly influenced by the interaction of several factors, including the back-to-back distance of the two channels, depth-to-width ratios, number of battened, and overall column slenderness ratios.**

***Keywords*- Finite Element Modeling, battened columns, back-to-back channels, Built-up column, Flexural buckling, Cold-formed steel, uniaxial loading, Direct Strength Method**

## I. INTRODUCTION

Recently, there has been an increase in the use of cold-formed steel (CFS) sections for various structural applications, largely due to their advantageous weight-to-strength ratios. This characteristic opens up opportunities for innovation and improved efficiency in construction processes. It also simplifies installation and fabrication while enabling the selection of cost-effective and efficient cross-sections [1-4]. Moreover, CFS sections are convenient and economical to handle and transport [5–6].

To enhance the structural performance of CFS built-up sections, chord elements are connected with lacings or battens along their lengths. These built-up sections are commonly used as columns to support significant axial and uniaxial loads. However, depending on the loading conditions, CFS members may experience different types of instability, including distortional buckling, flexural or overall (global) buckling, lateral-torsional buckling, and local buckling. Geometric imperfections can significantly affect the performance and ultimate capacity of CFS sections, as well as the effectiveness of strengthening measures [7-9].

Ongoing advancements in the development of design codes and recommendations for CFS structures have been driven by extensive research into improving the performance of CFS sections. Numerical simulations and experimental studies have been conducted on columns made from channel sections arranged in back-to-back and face-to-face configurations, often joined with batten plates connected by bolted, welded, or self-drilling screws [10-13].

Local web buckling in CFS sections with lower sectional compactness can be addressed using dividers between channel sections in built-up columns [14]. A detailed investigation is needed to determine the optimal spacer spacing for these types of columns. Laced built-up columns tend to offer superior axial strength and stability compared to battened columns, thanks to their continuous lateral connectivity [15]. Previous experimental studies on the cold-formed axial strength of built-up columns have been limited by a narrow range of geometric parameters [16-19]. The design strengths suggested by the Eurocode (EC3) [20] and North American specifications (NAS) [21] for short CFS built-up columns with lateral ties have often been considered overly conservative [22-25].

The novelty of this work lies in addressing the gap in research regarding the behaviour of channel built-up sections (CFS) under compression loads. While there has been extensive study on these members, there remains a limited investigation into their performance under varying levels of sectional

Journal of Engineering Research (JER)
ISSN: 2356-9441 Vol. 9 – No. 1, 2025 ©Tanta University, Faculty of Engineering e ISSN: 2735-4873

compactness, section slenderness, and unbraced chord slenderness. Therefore, this study is crucial in exploring the effects of back-to-back spacing and slenderness ratio on the axial compression and eccentric load performance of built-up columns, considering different sectional dimensions. Additionally, the work aims to evaluate the adequacy of current design standards in accurately predicting the uniaxial strengths of CFS battened built-up columns.

## II. Finite Element Model

### A. *Modeling techniques*

ABAQUS [26] was used to develop a numerical model simulating the behavior of a CFS battened column, accounting for both its elastic and plastic behavior. The following analysis section outlines the model's geometry and material properties. The goal of this model is to provide a reliable simulation of the performance of battened columns made from built-up cold-formed steel (BCFS). The self-drilling screws were modeled with the CONN3-D2 element, a three-dimensional beam connector with two nodes and six degrees of freedom per node [29, 30], as illustrated in Figure 1.

Buckling analysis using finite element methods is conducted in two stages. The first stage involves determining the buckling modes of the columns through Eigenvalue analysis. This linear elastic analysis uses the (*BUCKLE) command from the ABAQUS library, with the load applied in a specified step. Multiple buckling modes are evaluated, and the most relevant mode, as predicted by the Eigenvalue analysis, is selected. In the parametric study, the reference points are located at the column ends.

The second stage is a nonlinear load-displacement analysis that incorporates initial imperfections and material nonlinearity. This stage provides a detailed assessment of ultimate loads, failure modes, lateral displacements, axial strains, and axial shortenings.

### B. *Batten plates and chords of the channel*

The S4R shell element is used to model the channels (chords) of slender cold-formed steel sections and batten plates. This element provides an accurate solution for most applications, with six degrees of freedom per node. The mesh was selected to ensure sufficient accuracy while minimizing computational time for modeling steel sections in cold-formed battened columns. To achieve this, an approximate global area of 25 $mm^2$ was chosen for elements sized 5 mm × 5 mm. A finer mesh was applied to the corner regions of the chord members for greater precision.

### C. *Loading plates*

The model incorporates rigid upper and lower-end plates. The finite element analysis was performed using a three-dimensional (3D) mesh with four-node bilinear rigid quadrilateral shell elements (R3D4), as shown in Figure 1. For each specimen, a reference point (RP) was selected perpendicular to the plane of each end plate and directed toward the center of the plate, using the effective length between the pin ends. This reference point (RP) handled the boundary conditions, while the RP at the upper-end plate was responsible for applying the load. Figure 1 illustrates how a multipoint constraint (MPC) was used to link all degrees of freedom from the reference points (RP) to the column end nodes, simulating a rigid end-bearing plate.

A "Tie" constraint was used to connect the loading plate to the cold-formed steel channels, preventing rotations and displacements of the elements during loading. In ABAQUS, this tie constraint automatically combines the three-dimensional shell meshes.

### D. *Characteristics of materials*

Experimental testing is essential for determining the material properties of the steel. For slender sections, the maximum stress mustn't exceed the yield stress. In finite element analysis, the stress-strain relationship is often simplified and approximated as bilinear or idealized for ease of modeling. This approximation is applied to the cross-section of the material. However, ABAQUS offers the flexibility to use a multilinear stress-strain curve, enhancing its capability to model various material behaviors.

In this parametric study, the properties of carbon steel were considered. The steel was modeled using von Mises isotropic hardening with a minimum yield stress ($F_y$) of 355 MPa and an ultimate strength ($F_u$) of 510 MPa. The shear modulus was set at 81,000 MPa. The bilinear elastic-plastic stress-strain curve with linear strain hardening was applied for the simulation. The linear elastic part of the curve was characterized by a Young's modulus ($E_0$) of 210 GPa and a Poisson's ratio of 0.3. In the nonlinear analysis, plastic hardening was incorporated into the model using the von Mises criterion, expanding the isotropic yield surface.

### E. *Boundary conditions and loads*

The following is a breakdown of the structural analysis setup for columns with hinged ends.

1. Hinged Ends on CFS Battened Columns where the ends are hinged, meaning they allow rotation but no translation. This is crucial for modeling how the column behaves under different loading conditions.

2. Displacements and Rotations at Reference Points (RPs): Boundary conditions are applied at specific reference points (RPs) on the column to simulate these hinged ends. The displacements (translations) and rotations at these points are constrained in certain directions. The upper RP restricts translations along the X and Y axes and rotation about the Z-axis, while the lower RP has restrictions on all translations (X,



https://digitalcommons.aaru.edu.jo/erjeng/vol9/iss1/19
DOI: https://doi.org/10.70259/engJER.2025.911910

Journal of Engineering Research (JER)
ISSN: 2356-9441 Vol. 9 – No. 1, 2025 ©Tanta University, Faculty of Engineering e ISSN: 2735-4873

Y, Z) and rotation about the Z-axis.

3. Modified RIKS Technique in ABAQUS: using a nonlinear analysis method (Modified RIKS) within ABAQUS to incrementally apply the load and track the column's response, especially when dealing with large deformations. This method is useful for capturing post-buckling behavior and complex load paths.

4. Column Subjected to Beginning Moments ($M_{uy} = P_u * e_x$): The column is subjected to moments generated by an eccentric axial load. The term ($M_{uy} = P_u * e_x$) suggests the creation of a bending moment due to the eccentricity ($e_{x)}$ (the distance along the X-axis from the centerline of the column to the line of action of the axial load ($P_u$).

The structural column is modeled under axial load with an eccentricity that generates bending. The boundary conditions reflect how the column is constrained at both ends to simulate hinged supports, and the Modified RIKS technique is used to capture the behavior under these loading conditions.

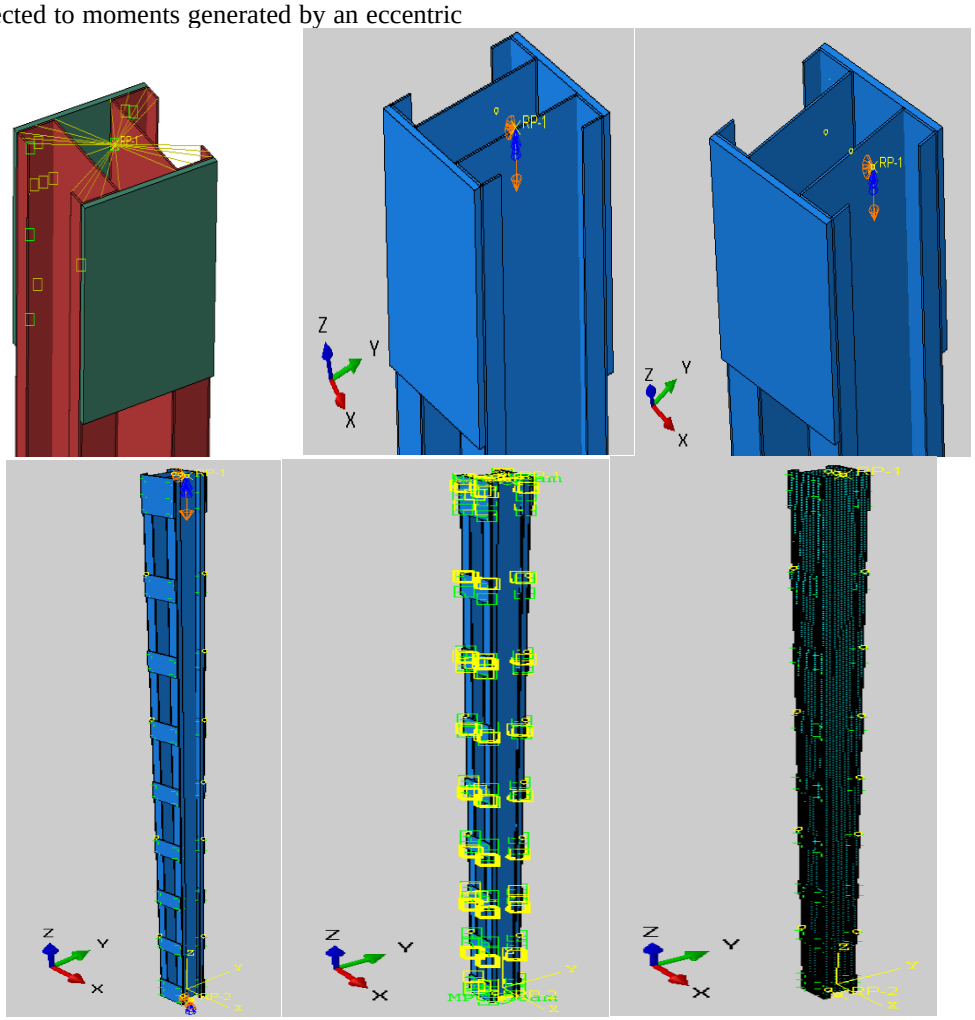


**Figure1. Finite elements mesh, load application Fastener modeling, and Boundary conditions**

Journal of Engineering Research (JER)
ISSN: 2356-9441 Vol. 9 – No. 1, 2025 ©Tanta University, Faculty of Engineering e ISSN: 2735-4873

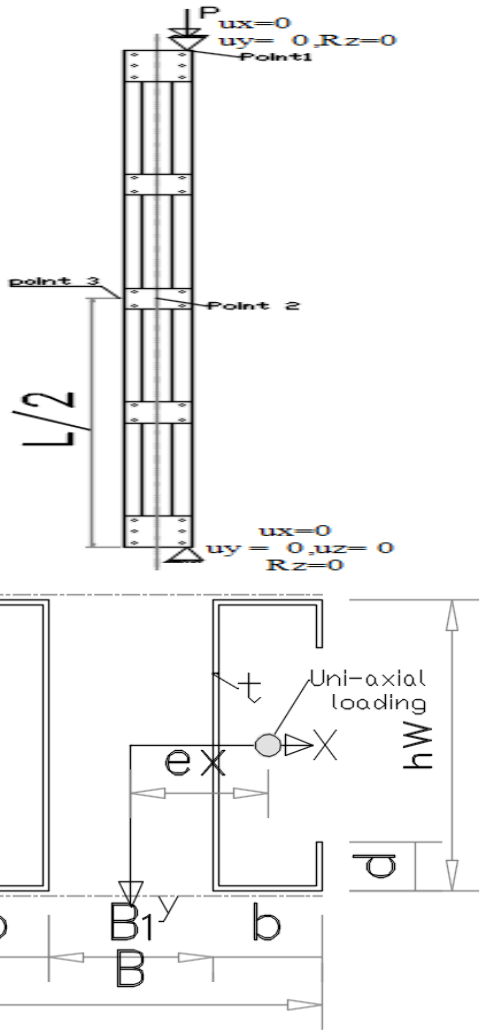


**Figure2. Loading positions at column upper loaded end and support position at column lower support end for column subjected to Uni-axial loads**

.

## F. *Initial geometric imperfections*

The finite elements analysis considers the observed magnitudes of both failure modes: local buckling and overall buckling. Eigenvalue analyses of the column are performed to identify these buckling modes and establish the initial overall imperfections. According to the literature review [27-28], the average overall imperfections for the tested specimens were found to be 1/1000 of the total length of the specimen. These overall imperfections were simulated for battened columns made from cold-formed steel sections. All buckling modes predicted by the ABAQUS Eigenvalue analysis are normalized to 1.0, and the measured magnitudes of the initial local and overall geometric imperfections are incorporated into the buckling modes.

## G. *Verification of Finite Element Model*

The nonlinear finite element model of the CFS open-section battened column, developed using ABAQUS [26], was calibrated against experimental data from previous studies [27, 28].

The experimental investigations of Dabaon et al. [27] focused on axially loaded built-up columns consisting two cold-formed steel channels placed back-to-back connected by batten plates with different longitudinal spacing. The column strengths, failure modes, load-lateral displacement, and load-axial shortening relationships predicted numerically were compared against those measured experimentally, as summarized in Table 1 and presented in Figs. 3. The column strengths obtained in the tests ($P_{Test}$) and finite element analysis ($P_{FE}$) were compared, as shown in Table 1 and presented in Figs. 3.

El-Aghoury et al. [28] investigated a series of four equal slender angles subjected to uniaxial bending moments. The test specimens were made by connecting four CFS angle sections with batten plates. The column strengths obtained in the tests ($P_{Test}$) and finite element analysis ($P_{FE}$) were compared, as shown in Table 1 and presented in Figs. 4.

The CFS battened column finite element (FE) model was accomplished to be compared with the test results from these studies [27, 28]. Both failure modes and load-versus-lateral displacement curves were confirmed. Figures 3 and 4 display the load-lateral displacement, axial shortening, and failure modes. Table 1 compares the FEA and experimental ultimate capacities for Cold-Formed Steel (CFS) battened columns [27, 28].

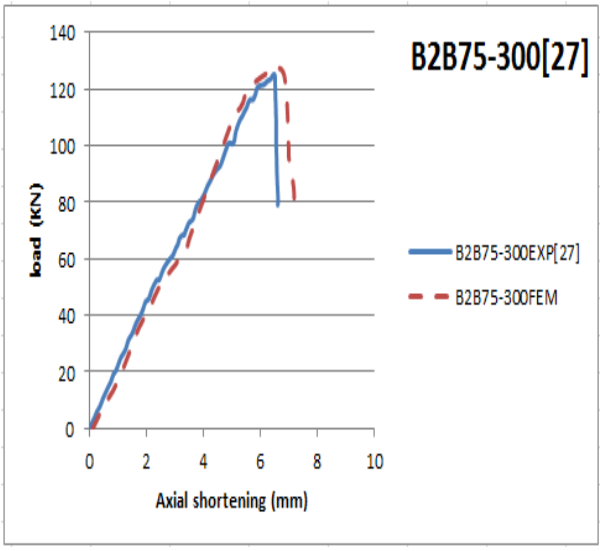


**A) Axial shortening-load relationships**



https://digitalcommons.aaru.edu.jo/erjeng/vol9/iss1/19
DOI: https://doi.org/10.70259/engJER.2025.911910

Journal of Engineering Research (JER)
ISSN: 2356-9441 Vol. 9 – No. 1, 2025 ©Tanta University, Faculty of Engineering e ISSN: 2735-4873

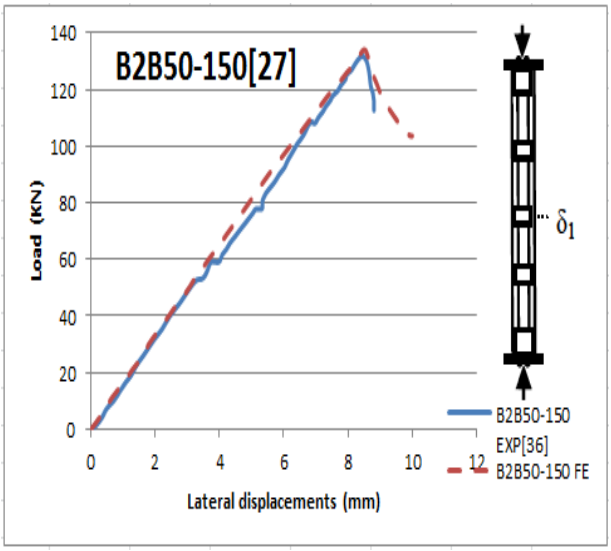


B) Lateral displacement-load relationships

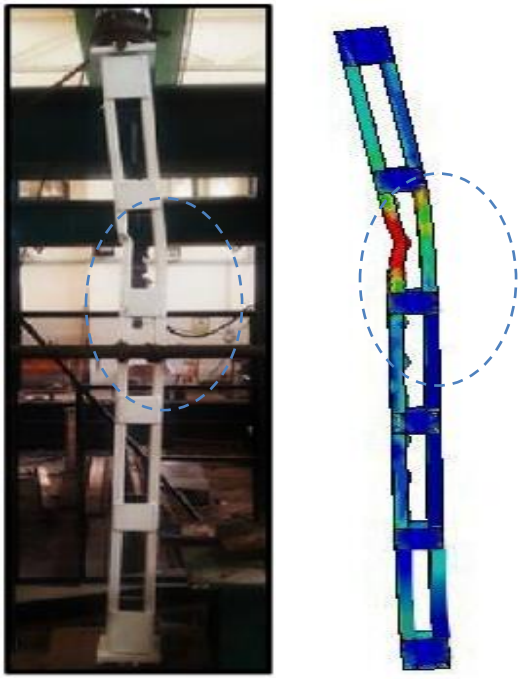

B2B75-300[27]

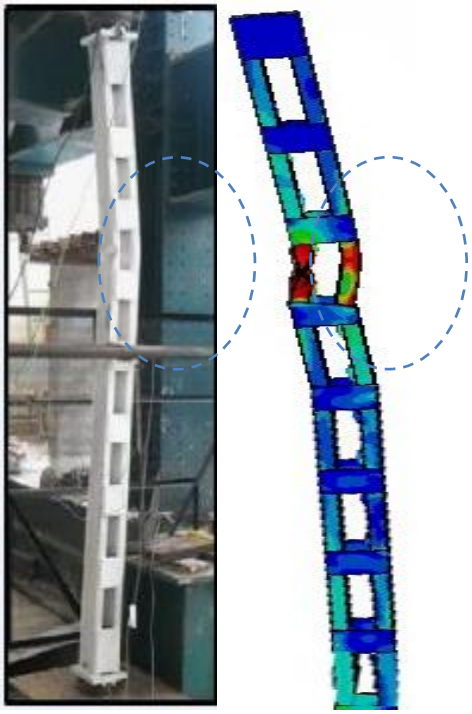

B2B50-150[27]

C) Comparison of the modes of failure between test specimens and the finite models of [27]

Fig. 3. (A): Lateral displacement-load relationships, (B): Axial shortening, and (C): failure modes
Flexural buckling (FB) and local buckling (LB)

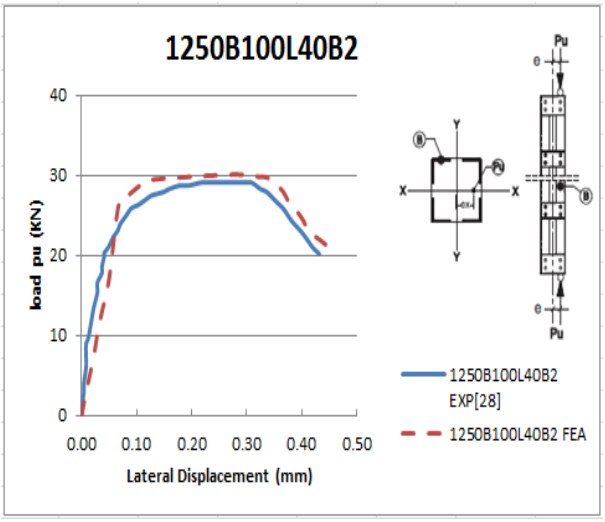

Journal of Engineering Research (JER)
ISSN: 2356-9441 Vol. 9 – No. 1, 2025 ©Tanta University, Faculty of Engineering e ISSN: 2735-4873

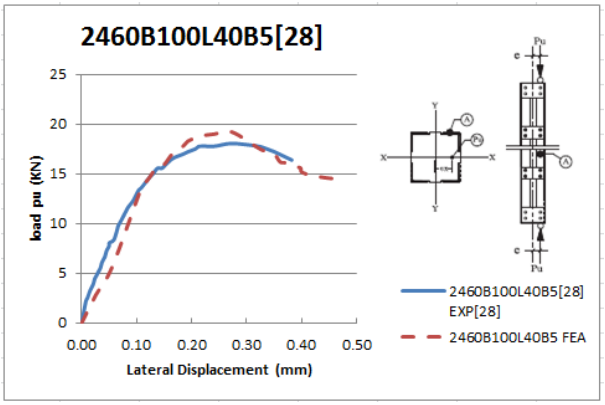


A) Lateral displacement-load relationships

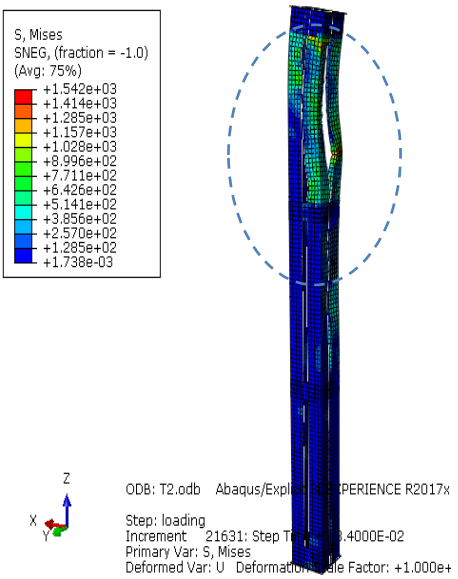


B) Modes of failure shape of (1250B100L40B2) [28]

**Fig. 4. (A): Lateral displacement-load relationships, and (B): failure modes flexural–torsional Flexural buckling (coupled), flexural/flexural-torsional (FT)**

**Table1. Battened column Strength of the FEA and experimental test [27, 28]**

| Specimen | Load type | Load Ecc. | | Exp. Results | | $F_{EA}$ Results | | $P_{test}/P_{F.E.A}$ |
|---|---|---|---|---|---|---|---|---|
| | | $e_x$ mm | $e_y$ mm | $P_{test}$ (kN) | Failure mode | $P_{F.E.A}$ (kN) | Failure mode | |
| B2B75–300 [27] | Axially load | - | - | 125.2 | LB | 126.5 | LB | 0.989 |
| B2B50–150 [27] | Axially load | - | - | 133.12 | FB | 134 | FB | 0.993 |
| 1250B100L40B2 [28] | Uni-axially | 30 | - | 28.2 | FT | 30 | FT | 0.933 |
| 2460B100L40B5[28] | Uni-axially | 30 | | 18 | coupled | 19.6 | Coupled | 0.918 |

The comparison of FEA results with test results across the four aspects—strengths, failure modes, axial shortening, and the load vs. displacement relationship—shows strong agreement. Therefore, the FE model is considered suitable for the intended parametric study.

## *H. Parametric study overview*

The parametric study analyzed 48 built-up cold-formed steel battened columns with varying apparent distances between the two channels (B1) and buckling lengths (L and Lz), as illustrated in Figure 5. Column dimensions are depicted in Figure 5 and detailed in Table 2. The columns had lengths of 2400, 3000, and 5800 mm and were categorized into four series, each with a back-to-back unobstructed distance (B1) of 40, 60, 80, and 90 mm. These series were subjected to uniaxial loading. The channel cross-section in (mm), hw × b × d× t; 120×40×20×2mm.

The buckling lengths (Lz) of single channels in each group were 600, 460, 450, 340, 250, and 175 mm. The corresponding slenderness ratios of the channels between batten plates (λz) were 38.7, 29.67, 29.03, 21.93, 16.12, and 11.29, respectively. The overall slenderness ratio (λ = L/r_min) of the columns, calculated according to AISI S-100:2016 [21], ranged from 50 to 162. The load eccentricities (U) ranged from 20 to 68 mm.

## Specimen Labeling

The specimens were labeled as LB1-LzUex, with an example label being "2400B40-450U20."

**L**: Column length – 2400 mm

**B40:** Indicates a 40 mm distance between the two channels in the built-up section (B1 = 40 mm).



https://digitalcommons.aaru.edu.jo/erjeng/vol9/iss1/19
DOI: https://doi.org/10.70259/engJER.2025.911910

Journal of Engineering Research (JER)
ISSN: 2356-9441 Vol. 9 – No. 1, 2025 ©Tanta University, Faculty of Engineering e ISSN: 2735-4873

- **U20**: Indicates uniaxial loading with a 20 mm eccentricity in the x-direction from the center of gravity.
- **450:** Denotes the buckling length (Lz) of a single channel along its minor axis, measured as 450 mm.

The ultimate strengths ($P_{UFE}$), modes of failure, and non-dimensional critical slenderness (λc) of the columns, as determined using North American specifications [21], are summarized in Table 3. The results were derived from the analyses of the finite element model developed for the built-up cold-formed steel battened columns.

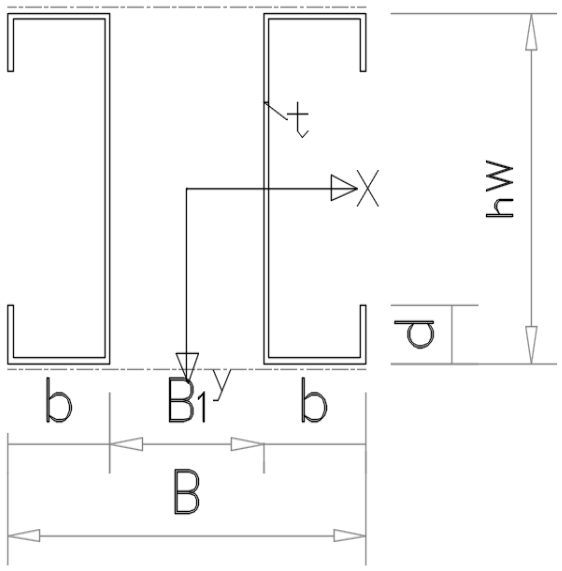


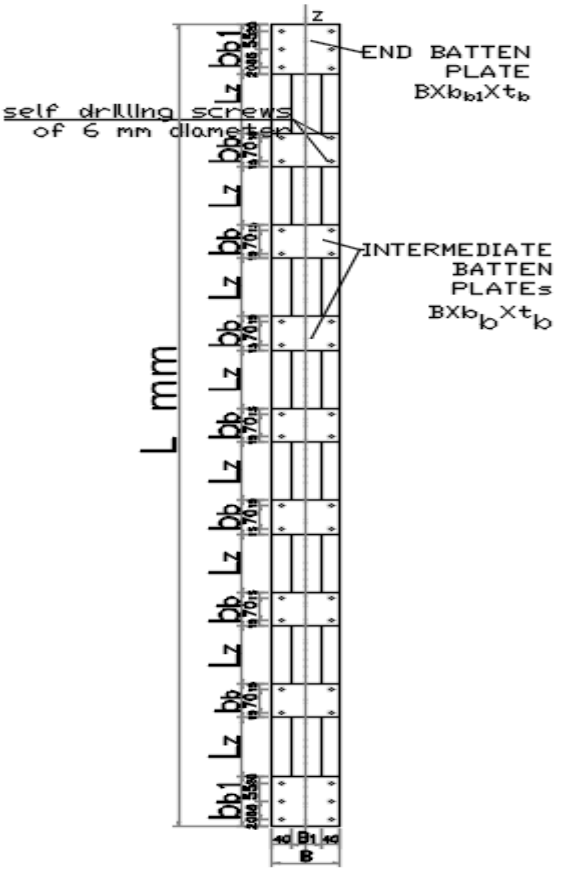


**Fig.5.The cross-sectional dimensions analyzed in the parametric study.**

**Table 2. The parametric study's specimen dimensions.**

| Series | Specimen | L (mm) | Lz (mm) | B1/hw | $\lambda_z$ | $\lambda = L/r_{min}$ | Load ccentricity $e_x$ (mm | Batten plates' dimensions i (mm) | | |
|---|---|---|---|---|---|---|---|---|---|---|
| | | | | | | | | $b_b$ | $b_{b1}$ | $t_b$ |
| B40 | 2400B40-450U20 | 2400 | 450 | 0.33 | 29.032 | 71.29 | 20 | 100 | 150 | 6 |
| | 2400B40-450U48 | 2400 | 450 | 0.33 | 29.032 | 71.29 | 48 | 100 | 150 | 6 |
| | 2400B40-340U20 | 2400 | 340 | 0.33 | 21.935 | 68.71 | 20 | 100 | 150 | 6 |
| | 2400B40-340U48 | 2400 | 340 | 0.33 | 21.935 | 68.71 | 48 | 100 | 150 | 6 |
| | 2400B40-175U20 | 2400 | 175 | 0.33 | 11.29 | 66.08 | 20 | 100 | 150 | 6 |
| | 2400B40-175U48 | 2400 | 175 | 0.33 | 11.29 | 66.08 | 48 | 100 | 150 | 6 |
| | 3000B40-600U20 | 3000 | 600 | 0.33 | 38.70 | 90.20 | 20 | 100 | 150 | 6 |
| | 3000B40-600U48 | 3000 | 600 | 0.33 | 38.70 | 90.20 | 48 | 100 | 150 | 6 |
| | 3000B40-460U20 | 3000 | 460 | 0.33 | 29.67 | 86.60 | 20 | 100 | 150 | 6 |
| | 3000B40-460U48 | 3000 | 460 | 0.33 | 29.67 | 86.60 | 48 | 100 | 150 | 6 |
| | 3000B40-250U20 | 3000 | 250 | 0.33 | 16.12 | 82.90 | 20 | 100 | 150 | 6 |

Journal of Engineering Research (JER)
ISSN: 2356-9441 Vol. 9 – No. 1, 2025 ©Tanta University, Faculty of Engineering e ISSN: 2735-4873

| | | | | | | | | | | |
|---|---|---|---|---|---|---|---|---|---|---|
| | 3000B40-250U48 | 3000 | 250 | 0.33 | 16.12 | 82.90 | 48 | 100 | 150 | 6 |
| | 5800B40-600U20 | 5800 | 600 | 0.33 | 38.70 | 162.1 | 20 | 100 | 150 | 6 |
| | 5800B40-600U48 | 5800 | 600 | 0.33 | 38.70 | 162.1 | 48 | 100 | 150 | 6 |
| | 5800B40-460U20 | 5800 | 460 | 0.33 | 29.67 | 160.1 | 20 | 100 | 150 | 6 |
| | 5800B40-460U48 | 5800 | 460 | 0.33 | 29.67 | 160.1 | 48 | 100 | 150 | 6 |
| | 5800B40-250U20 | 5800 | 250 | 0.33 | 16.12 | 158.1 | 20 | 100 | 150 | 6 |
| | 5800B40-250U48 | 5800 | 250 | 0.33 | 16.12 | 158.1 | 48 | 100 | 150 | 6 |
| B60 | 2400B60-450U30 | 2400 | 450 | 0.5 | 29.032 | 59.60 | 30 | 100 | 150 | 6 |
| | 2400B60-450U56 | 2400 | 450 | 0.5 | 29.032 | 59.60 | 56 | 100 | 150 | 6 |
| | 2400B60-340U30 | 2400 | 340 | 0.5 | 21.935 | 56.49 | 30 | 100 | 150 | 6 |
| | 2400B60-340U56 | 2400 | 340 | 0.5 | 21.935 | 56.49 | 56 | 100 | 150 | 6 |
| | 2400B60-175U30 | 2400 | 175 | 0.5 | 11.29 | 53.27 | 30 | 100 | 150 | 6 |
| | 2400B60-175U56 | 2400 | 175 | 0.5 | 11.29 | 53.27 | 56 | 100 | 150 | 6 |
| | 3000B60-600U30 | 3000 | 600 | 0.5 | 38.70 | 75.71 | 30 | 100 | 150 | 6 |
| | 3000B60-600U56 | 3000 | 600 | 0.5 | 38.70 | 75.71 | 56 | 100 | 150 | 6 |
| | 3000B60-460U30 | 3000 | 460 | 0.5 | 29.67 | 71.52 | 30 | 100 | 150 | 6 |
| | 3000B60-460U56 | 3000 | 460 | 0.5 | 29.67 | 71.52 | 56 | 100 | 150 | 6 |
| | 3000B60-250U30 | 3000 | 250 | 0.5 | 16.12 | 67.04 | 30 | 100 | 150 | 6 |
| | 3000B60-250U56 | 3000 | 250 | 0.5 | 16.12 | 67.04 | 56 | 100 | 150 | 6 |
| | 5800B60-600U30 | 5800 | 600 | 0.5 | 38.70 | 131.6 | 30 | 100 | 150 | 6 |
| | 5800B60-600U56 | 5800 | 600 | 0.5 | 38.70 | 131.6 | 56 | 100 | 150 | 6 |
| | 5800B60-460U30 | 5800 | 460 | 0.5 | 29.67 | 129.2 | 30 | 100 | 150 | 6 |
| | Specimen | L (mm) | Lz (mm) | B1/hw | λz | $\lambda = L/r_{min}$ | Load Eccentricity $e_x$ (mm) | Batten plates' dimensions in (mm) | | |
| | | | | | | | | $b_b$ | $b_{b1}$ | $t_b$ |
| | 5800B60-460U56 | 5800 | 460 | 0.5 | 29.67 | 129.26 | 56 | 100 | 150 | 6 |
| | 5800B60-250U30 | 5800 | 250 | 0.5 | 16.12 | 126.84 | 30 | 100 | 150 | 6 |
| | 5800B60-250U56 | 5800 | 250 | 0.5 | 16.12 | 126.84 | 56 | 100 | 150 | 6 |
| B80 | 2400B80-450U40 | 2400 | 450 | 0.67 | 29.03 | 51.99 | 40 | 100 | 150 | 6 |
| | 2400B80-450U64 | 2400 | 450 | 0.67 | 29.03 | 51.99 | 64 | 100 | 150 | 6 |
| | 2400B80-340U40 | 2400 | 340 | 0.67 | 21.93 | 51.94 | 40 | 100 | 150 | 6 |
| | 2400B80-340U64 | 2400 | 340 | 0.67 | 21.93 | 51.94 | 64 | 100 | 150 | 6 |
| | 2400B80-175U40 | 2400 | 175 | 0.67 | 11.29 | 51.94 | 40 | 100 | 150 | 6 |
| | 2400B80-175U64 | 2400 | 175 | 0.67 | 11.29 | 51.94 | 64 | 100 | 150 | 6 |
| B90 | 2400B90-450U45 | 2400 | 450 | 0.75 | 29.03 | 51.94 | 20 | 100 | 150 | 6 |
| | 2400B90-450U68 | 2400 | 450 | 0.75 | 29.03 | 51.94 | 48 | 100 | 150 | 6 |



https://digitalcommons.aaru.edu.jo/erjeng/vol9/iss1/19
DOI: https://doi.org/10.70259/engJER.2025.911910

Journal of Engineering Research (JER)
ISSN: 2356-9441 Vol. 9 – No. 1, 2025 ©Tanta University, Faculty of Engineering e ISSN: 2735-4873

| | | | | | | | | | | |
|---|---|---|---|---|---|---|---|---|---|---|
| | 2400B90-340U45 | 2400 | 340 | 0.75 | 21.93 | 51.94 | 20 | 100 | 150 | 6 |
| | 2400B90-340U68 | 2400 | 340 | 0.75 | 21.93 | 51.94 | 48 | 100 | 150 | 6 |
| | 2400B90-175U45 | 2400 | 175 | 0.75 | 11.29 | 51.94 | 20 | 100 | 150 | 6 |
| | 2400B90-175U68 | 2400 | 175 | 0.75 | 11.29 | 51.94 | 48 | 100 | 150 | 6 |

$e_x$: The eccentric distance along X-axis is equivalent to (0.5B1&0.4B) from the C. G. of the section

## III. Design Method

### *A. Design rules following North American code (AISI S-100:2016) [21]*

The design code NAS [21] presents two primary design methodologies: The Direct Strength Method (DSM) and the Effective Width Method (EWM). Accurately estimating the elastic critical buckling stress is a key factor influencing the precision and reliability of the DSM.

**Built-up sections**

For built-up compression members, the axial strength shall be determined following section E2 subjected to the following modifications.

$$\left(\frac{KL}{r}\right)_m = \sqrt{\left(\frac{kl}{r}\right)_o^2 + \left(\frac{L_Z}{r_i}\right)^2} \quad (1)$$

Where:

$\left(\frac{kl}{r}\right)_o$ = overall slenderness ratio of the entire section about the built-up member axis

$L_Z$ = Intermediate fastener or spot weld spacing

$r_i$ = minimum radius of gyration of the full unreduced cross-sectional area of individual shapes of built-up sections.

**Uni-axially loaded column**

• Calculation method in AISI S100-16

$$\frac{\bar{P}}{Pn} + \frac{\bar{M}y}{Mny} \leq 1.0 \quad (2)$$

$$\bar{M}_y = B_1 \, e \, \bar{P} \quad (3)$$

$$B_1 = Cm / (1 - \alpha \, \bar{P} / P_{el}) \geq 1.0 \quad (4)$$

$$P_{el} = \pi^2 \, E \, I_y / (K_y \, L_y)^2 \quad (5)$$

Nominal flexural strength for lateral-torsional buckling as per the DSM

for $M_{cre} < 0.56 \, M_y$ (6)

$M_{ne} = M_{cre}$

for $2.78M_y \geq M_{cre} \geq 0.56M_y$

$M_{ne} = 10 / 9 \, M_y \, (1 - 10M_y / 36M_{cre})$ (7)

for $M_{cre} > 2.78M_y$

$M_{ne} = M_y$ (8)

$$M_{nl} \quad M_{ne} \quad \lambda 1 \leq 0.776 \quad (9)$$

for

$M_{ne} \, [1 - 0.15 \, (M_{crl} / M_{ne})^{0.4}] \, (M_{crl} / M_{ne})^{0.4}$

For $\lambda 1 > 0.776$ (10)

Nominal flexural strength of distortional buckling by the DSM

$$M_{nd} \quad S_F f_y \quad \begin{cases} \lambda_d \leq 0.673 \\ M_y \, [1 - 0.22 \, (M_{crd} / My)\text{^}0.5] \, (Mc_{rd} / My)\text{^}0.5 \end{cases} \quad (11)$$

for $\lambda_d >$ 0.673

$$M_{crd} = S_F \, F_{crd} \quad (12)$$

$$\lambda 1 = \sqrt{M_y / M_{cr1}}, \quad \lambda_d = \sqrt{M_y / M_{crd}} \quad (13)$$

Mn min (Mne, Mnl, Mnd)

Where $\bar{P}$ is the required compressive axial Strength; Pn is the available axial strength; Fcrd is the elastic distortional buckling stress calculated by Appendix2; Mcre is the critical elastic local buckling moment nominal flexural strength of local yielding by the DSM in accordance withAppendix2; $\bar{M}$ and M are the required flexural strength about the x- and y-axis, respectively, α =1, Cm= 0, e is the eccentricity, Sf is the gross section modulus referenced to the extreme fibre at first yield, Moreover, Mny is the available flexural strength about the y-axis.

### *B. Design regulations following the EN 1993-1-3:2006 [20]*

The un-factored design strength for class 4 is determined by EC3 (BS EN1993-1-3) as follows:

$$P_{EC3} = \chi \, A_e \, f_y \quad (14)$$

$$\chi = 1 / (\phi + \sqrt{(\phi^2 - \bar{\lambda}^2)}) \text{ for } \chi \leq 1.0 \quad (15)$$

$$\phi = 0.5[1 + \alpha \, (\bar{\lambda} - 0.2) + \bar{\lambda}^2] \quad (16)$$

$$\bar{\lambda} = \sqrt{(A_{eff} \, f_y / N_{cr})} = (L_{cr} / i) \sqrt{(A_e \, f_y / \lambda_1 \, A_g)} \quad (17)$$

for Class 4 cross-sections

$$\lambda_1 = \pi \sqrt{(E / f_y)} \quad (18)$$

Where:

χ: the applicable buckling mode reduction factor.
Ncr: refers to the critical force for elastic design associated with specific buckling mode
Ae: the effective cross-sectional area.
FY: A proof stress of 0.2% (σ 0.2) is the same as the yield stress.
"α" imperfection factor.

For a laterally unrestrained beam, the buckling resistance for

Journal of Engineering Research (JER)
ISSN: 2356-9441 Vol. 9 – No. 1, 2025 ©Tanta University, Faculty of Engineering e ISSN: 2735-4873

the design moment approximated calculated as Mb, Rd = $\chi_{LT}$ fy wy / $\gamma$M1 (19)

$$\chi_{LT} = 1 / (\phi_{LT} + \sqrt{(\phi_{LT}^2 - \bar{\lambda}_{LT}^2)}) \text{ for } \chi \leq 1.0$$

Where:
$\chi$ LT =lateral –torsional buckling reduction factor

Wy represents the suitable section modulus:
cross sections for class 4
$W_y = W_{eff,y}$;

$\gamma_{M1}$=partial factor =1

$$(N_{Ed} / N_{b,Rd})^{0.8} + (M_{Ed} / M_{b,Rd})^{0.8} \leq 1.0 \quad (20)$$

Where:
Mb, Rd: is the design buckle resistance moment;
MEd: is the design moment value.
Beam-column design by EN1993-1-1 and EN1993-1-3:
Nb, Rd: is the design buckling resistance of the compression member;
NEd: is the design value of compression force by EN1993-1-1 and EN1993-1-3.
Alternately, the interaction formula may be applicable:

## IV. Reliability analysis

A reliability study assessed the existing design criteria for cold-formed steel built-up battened columns. The reliability study was performed according to the ASCE Specifications Commentary [31]. The reliability index (β) ranges from 2.5 to 3.5 for cold-formed steel structural components. The design criteria are regarded as reliable if the reliability index exceeds 2.5. The load combination of 1.2DL + 1.6LL, with resistance factors (ϕ) of P= 0.85 and My= 0.95, was used to calculate the reliability index (β) for NAS [21] and EC3 [20] specifications, where DL denotes dead load and LL denotes live load. The statistical parameters (Mm = 1.10, Fm = 1.00, Vm = 0.10, and VF = 0.05) used in the calculation are obtained from the Commentary of the ASCE Specification for compression members.
The resistance factor of 0.85 was considered according to AISI S100 to calculate the Qm/Rn. A trustworthy design process has a reliability index greater than 2.5. The higher the reliability index, the more reliable the prediction. AISI S100:2016 provides equations to determine the reliability index (β).

$$\beta = \frac{In(M_m F_m P_m \frac{R_n}{Q_m}}{\sqrt{V_M^2 + V_F^2 + V_P^2 + V_Q^2}}$$

where:
Pm =Represent the Mean ratio of the finite element determined moment to the predicted moment for the design codes and Vp are the corresponding COVs
Mm = Mean ratio of the actual yield stress to the minimum specified value.
Fm = Mean ratio of the actual section modulus to the specified (nominal) value.
VQ is also the mean load effect variation coefficient, which can be computed from the load ratio (in this study, 0.21)

**Table 3. Comparison of FEM results with the design codes' ultimate column strength**

| Series | Specimen name | FE Results | | Design strength | | | | FE/Design | |
|---|---|---|---|---|---|---|---|---|---|
| | | $Pu_{FE}$ (KN) | Failure Mode | $P_{NAS}$ (KN) | λc | $P_{EC3}$ (KN) | $\bar{\lambda}$ | $Pu_{FE}$ / $P_{NAS}$ | $Pu_{FE}$ /$P_{EC3}$ |
| B40 | 2400B40-450U20 | 151.08 | F+D+LTB | 126.4 | 0.93 | 119.4 | 0.85 | 1.193 | 1.265 |
| | 2400B40-450U48 | 100.45 | F+D+LTB | 83.4 | 0.93 | 77.1 | 0.85 | 1.204 | 1.302 |
| | 2400B40-340U20 | 153.05 | F+ D+ L | 128.1 | 0.89 | 119.4 | 0.85 | 1.194 | 1.281 |
| | 2400B40-340U48 | 102.54 | F+ L | 84.1 | 0.89 | 77.1 | 0.85 | 1.218 | 1.330 |
| | 2400B40-175U20 | 157.48 | F+ D+ L | 129.6 | 0.86 | 119.4 | 0.85 | 1.215 | 1.321 |
| | 2400B40-175U48 | 108.3 | F+LTB | 84.8 | 0.86 | 77.1 | 0.85 | 1.277 | 1.405 |
| | 3000B40-600U20 | 112 | F+L+LTB+D | 106.0 | 1.17 | 100.6 | 1.06 | 1.056 | 1.113 |
| | 3000B40-600U48 | 75.9 | F+L+D+LTB | 72.9 | 1.17 | 68.35 | 1.06 | 1.040 | 1.110 |
| | 3000B40-460U20 | 119 | F+L+D+LTB | 108.2 | 1.13 | 100.6 | 1.06 | 1.099 | 1.182 |
| | 3000B40-460U48 | 77.2 | F+L+D+LTB | 74.0 | 1.13 | 68.35 | 1.06 | 1.043 | 1.129 |



https://digitalcommons.aaru.edu.jo/erjeng/vol9/iss1/19
DOI: https://doi.org/10.70259/engJER.2025.911910

Journal of Engineering Research (JER)
ISSN: 2356-9441 Vol. 9 – No. 1, 2025 ©Tanta University, Faculty of Engineering e ISSN: 2735-4873

| | | | | | | | | | |
|---|---|---|---|---|---|---|---|---|---|
| | 3000B40-250U20 | 122.3 | F+ L+ D | 110.3 | 1.08 | 100.6 | 1.06 | 1.108 | 1.215 |
| | 3000B40-250U48 | 79.8 | F+ L+ D | 75.0 | 1.08 | 68.35 | 1.06 | 1.063 | 1.167 |
| | 5800B40-600U20 | 41.927 | L+F+LTB | 40.1 | 2.12 | 38.75 | 2.05 | 1.043 | 1.081 |
| | 5800B40-600U48 | 31.53 | F+LTB | 31.0 | 2.12 | 30.83 | 2.05 | 1.015 | 1.022 |
| | 5800B40-460U20 | 43.08 | L+F+LTB | 41.3 | 2.09 | 38.75 | 2.05 | 1.042 | 1.111 |
| | 5800B40-460U48 | 33.74 | F+LTB | 32.7 | 2.09 | 30.83 | 2.05 | 1.032 | 1.094 |
| | 5800B40-250U20 | 44.93 | L+F+LTB | 42.4 | 2.07 | 38.7 | 2.05 | 1.058 | 1.159 |
| | 5800B40-250U48 | 35.76 | F+L+LTB | 34.4 | 2.07 | 30.8 | 2.05 | 1.039 | 1.159 |
| B60 | 2400B60-450U30 | 155.7 | F+LTB | 134.2 | 0.78 | 122.6 | 0.68 | 1.161 | 1.27 |
| | 2400B60-450U56 | 110.02 | L+F+D | 95.1 | 0.78 | 88.3 | 0.68 | 1.172 | 1.301 |
| | 2400B60-340U30 | 157.6 | F+D | 135.9 | 0.73 | 122.6 | 0.68 | 1.160 | 1.285 |
| | 2400B60-340U56 | 116.82 | D+L+F | 99.1 | 0.73 | 88.3 | 0.68 | 1.172 | 1.314 |
| | 2400B601750U30 | 163.4 | F+LTB | 137.4 | 0.69 | 122.6 | 0.68 | 1.189 | 1.332 |
| | 2400B60-175U56 | 122.9 | F+LTB+D | 100.0 | 0.69 | 88.3 | 0.68 | 1.229 | 1.391 |
| | 3000B60-600U30 | 119.23 | F+L+LTB+D | 117.3 | 0.99 | 105.7 | 0.85 | 1.016 | 1.128 |
| | 3000B60-600U56 | 91.64 | F+L+D+LTB | 88.0 | 0.99 | 78.72 | 0.85 | 1.041 | 1.164 |
| | 3000B60-460U30 | 119.6 | F+L+D+LTB | 118.6 | 0.93 | 105.7 | 0.85 | 1.008 | 1.131 |
| | 3000B60-460U56 | 93.37 | F+L+D+LTB | 88.7 | 0.93 | 78.7 | 0.85 | 1.052 | 1.186 |
| | 3000B60-250U30 | 124.9 | F+L+D+LTB | 121.0 | 0.87 | 105.7 | 0.85 | 1.031 | 1.181 |
| | 3000B60-250U56 | 95.6 | F+L+D | 90.4 | 0.87 | 78.7 | 0.85 | 1.05 | 1.214 |
| | 5800B60-600U30 | 62.38 | F+L | 50.31 | 1.72 | 48.2 | 1.64 | 1.239 | 1.292 |
| | 5800B60-600U56 | 51.1 | F+L | 42.89 | 1.72 | 40.8 | 1.64 | 1.191 | 1.252 |
| | 5800B60-460U30 | 64.93 | F+L+LTB | 52.78 | 1.69 | 48.2 | 1.64 | 1.230 | 1.345 |
| | 5800B60-460U56 | 53.4 | F+L+LTB | 44.64 | 1.96 | 40.8 | 1.64 | 1.196 | 1.308 |
| | 5800B60-250U30 | 67.39 | F+L | 54.79 | 1.66 | 48.27 | 1.64 | 1.229 | 1.396 |
| | 5800B60-250U56 | 55.08 | F+L | 46.05 | 1.66 | 40.8 | 1.64 | 1.196 | 1.350 |
| B80 | 2400B80-450U40 | 158.8 | F+LTB | 139.6 | 0.68 | 119.8 | 0.67 | 1.137 | 1.324 |
| | 2400B80-450U64 | 125.8 | F+L | 109.7 | 0.68 | 93.8 | 0.67 | 1.140 | 1.341 |
| | 2400B80-340U40 | 160.2 | F+LTB | 141.3 | 0.63 | 119.8 | 0.67 | 1.130 | 1.336 |
| | 2400B80-340U64 | 127.32 | F+L | 110. | 0.63 | 93.8 | 0.67 | 1.148 | 1.357 |
| | 2400B801750U40 | 165.3 | F+LTB | 139.6 | 0.67 | 119.8 | 0.67 | 1.180 | 1.379 |
| | 2400B80-175U64 | 132.32 | L+D | 109.8 | 0.67 | 93.8 | 0.67 | 1.200 | 1.410 |
| B90 | 2400B90-450U45 | 159.4 | L+F | 140.3 | 0.67 | 119.0 | 0.67 | 1.135 | 1.339 |
| | 2400B90-450U68 | 130.19 | LTB+L | 113.7 | 0.67 | 96.1 | 0.67 | 1.144 | 1.353 |

Journal of Engineering Research (JER)
ISSN: 2356-9441 Vol. 9 – No. 1, 2025 ©Tanta University, Faculty of Engineering e ISSN: 2735-4873

| | | | | | | | | | |
|---|---|---|---|---|---|---|---|---|---|
| | 2400B90-340U45 | 160.9 | F+D | 140.3 | 0.67 | 119.0 | 0.67 | 1.140 | 1.351 |
| | 2400B90-340U68 | 131.45 | F+L | 113.7 | 0.67 | 96.1 | 0.67 | 1.150 | 1.366 |
| | 2400B90-175U45 | 165.5 | L+F | 140.3 | 0.67 | 119. | 0.67 | 1.170 | 1.390 |
| | 2400B90-175U68 | 135.8 | L+LTB | 113.7 | 0.67 | 96.1 | 0.67 | 1.190 | 1.412 |
| Mean Pm = Average of the array(PFEM/Pcode) | | | | | | | | 1.133 | 1.263 |
| COV, VP | | | | | | | | 0.074 | 0.105 |
| Reliability index, β | | | | | | | | 3.32 | 3.545 |
| Resistance factor, Φ | | | | | | | | P=0.85&My=0.95 | |

L: local buckling
D: distortional buckling
LTB: lateral torsional buckling
F: flexural buckling

Table 3 compares the finite results with the design equations results for columns. The mean value and reliability index, according to DSM, are 1.133 and 3.32, but according to the EC3 interaction Equations, they are 1.263 and 3.545, respectively. Therefore, the current EC3(PEc3) predicts results that do not respect AISI specifications regarding the reliability index, while the Euro code buckling interaction DSM (PNas) predictions meet the NAS reliability requirement condition.

## V. Discussion of the results

### *A. Interaction curves*

Columns subjected to uniaxial loading, with varying channel slenderness ratios (λz) of 11.29, 16.12, 21.93, 29.03, 29.93, and 38.71 between batten plates, were analyzed for different column lengths and eccentricities. The interaction curves between normalized axial load ratios (Pu/Py) and moment ratios (Muy/My) were derived based on the results of the finite element analysis, as shown in Fig.6.

Column strength decreases with combined axial forces and moments, especially for higher slenderness ratios.

Shorter columns show higher normalized axial and moment ratios (Pu/Py and Muy/My) for the same slenderness ratios and back-to-back distances.

Reducing the slenderness ratio (λz) has minimal impact on strength for columns of the same length and back-to-back distance.

Increasing column length reduces load-bearing capacity.

The strength reduction due to combined axial and bending loads is more significant than for uniaxially loaded columns.

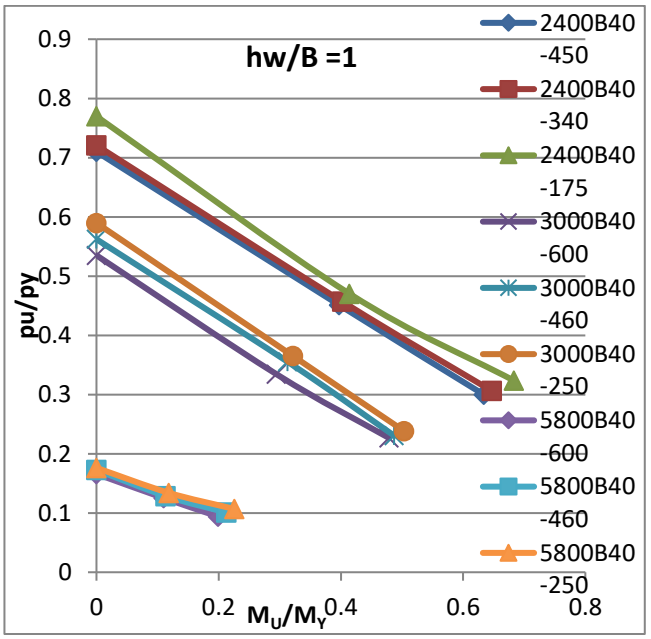


**Figure 6: Interaction relationship curves for uni-axially loaded column**

### *Comparison of the results obtained from FEA with the design codes.*

This section as shown in figure 7, 8, and 9 compares the finite element's ultimate strength with the design rules outlined in EC3 [20] and AISI [21]. This comparison is summarized in Table 3 for uniaxial loading. The maximum design compressive force was calculated by incorporating compressive load values and eccentricities into axial compressive force-bending moment interaction equations.

To ensure the strength of beam-column structures, the reliability index (β) was maintained within a range of 2.5 to 3.5, ensuring safe and reliable performance under varying loading conditions. This approach provides engineers with confidence in the adequacy of the design rules for achieving



https://digitalcommons.aaru.edu.jo/erjeng/vol9/iss1/19
DOI: https://doi.org/10.70259/engJER.2025.911910

Journal of Engineering Research (JER)
ISSN: 2356-9441 Vol. 9 – No. 1, 2025 ©Tanta University, Faculty of Engineering e ISSN: 2735-4873

sufficient safety margins.

Slenderness ratio (λz) significantly affects the strength of medium and slender battened columns, with higher λz causing notable strength reductions.

Uniaxially loaded columns showed linear behavior, with peak axial strength decreasing as λz increased. For example, at a length of 2400 mm, strength decreased by 18% when λz raised from 11.29 to 21.9 and by 30% when λz increased to 29.03.

AISI and EC3 design codes provided conservative predictions, with AISI having safety factors of 1.14–1.30 and EC3 having factors of 1.20–1.50. EC3 aligned more closely with finite element analysis (FEA), particularly for axial and uniaxial loads.

EC3 accounted for imperfections and effective widths, offering reliable predictions for medium-battened columns. AISI was more cautious for columns with uniaxial loads and eccentricity. Both codes generally yielded conservative results, with some cases showing strong agreement with FEA.

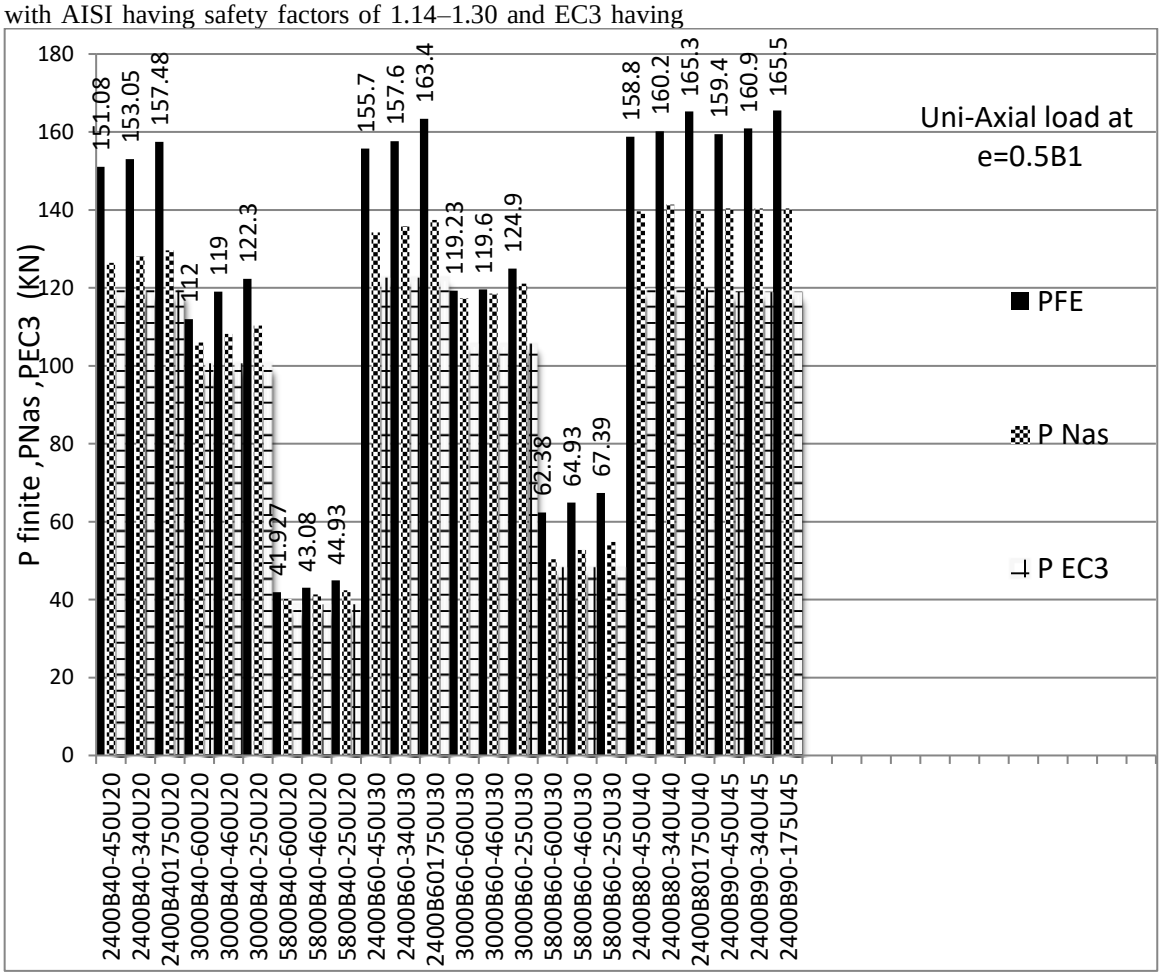

Journal of Engineering Research (JER)
ISSN: 2356-9441 Vol. 9 – No. 1, 2025 ©Tanta University, Faculty of Engineering e ISSN: 2735-4873

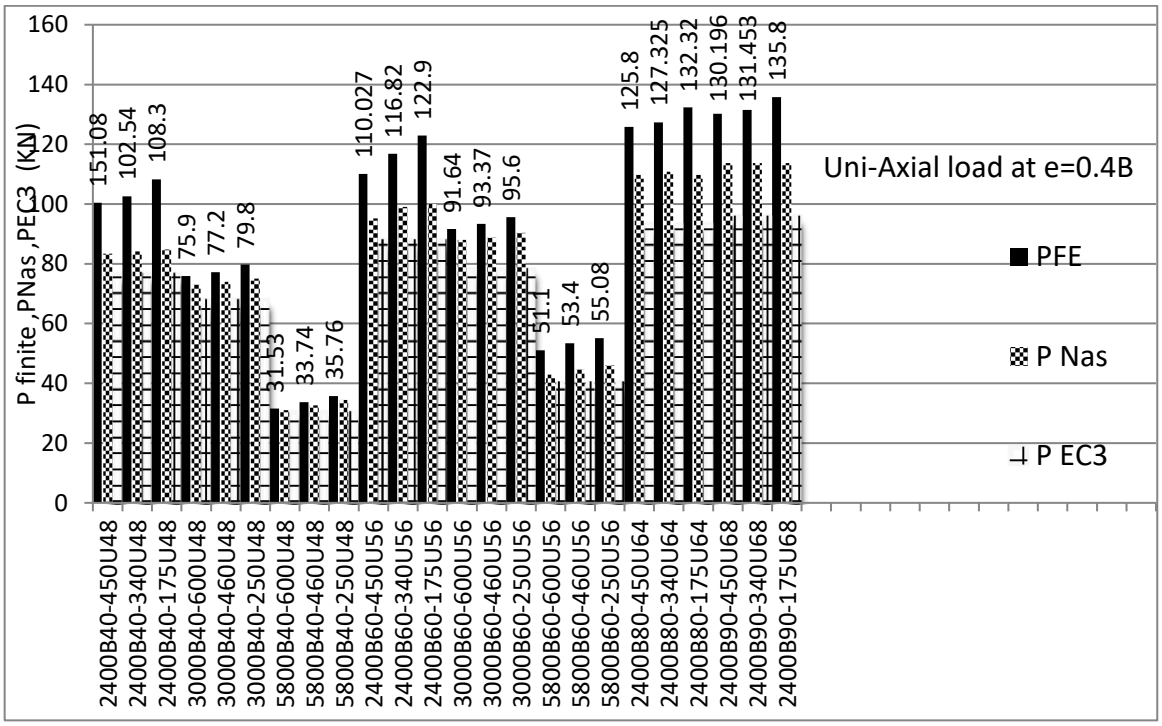


Figure 7: Comparison between FEA results with the design Code's strength

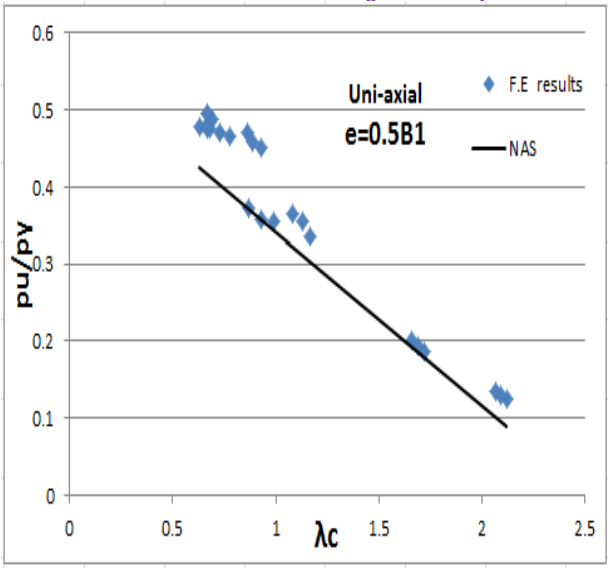


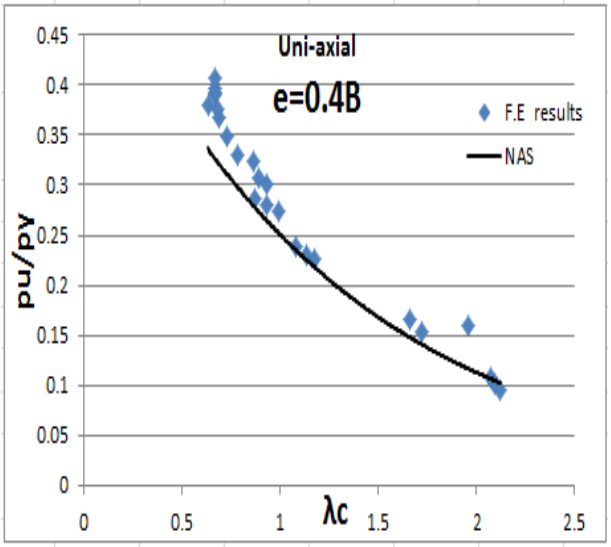


Fig. 8. The ratio of (pu/py) the normalized axial forces to the non-dimensional slenderness (λc) NAS [21]



https://digitalcommons.aaru.edu.jo/erjeng/vol9/iss1/19
DOI: https://doi.org/10.70259/engJER.2025.911910

Journal of Engineering Research (JER)
ISSN: 2356-9441 Vol. 9 – No. 1, 2025 ©Tanta University, Faculty of Engineering e ISSN: 2735-4873

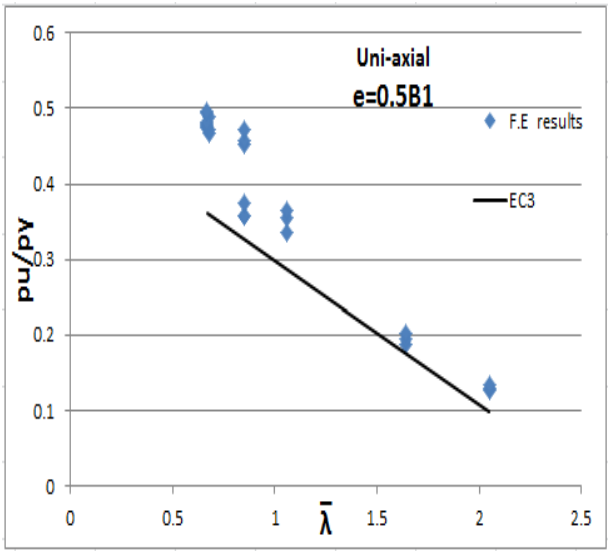


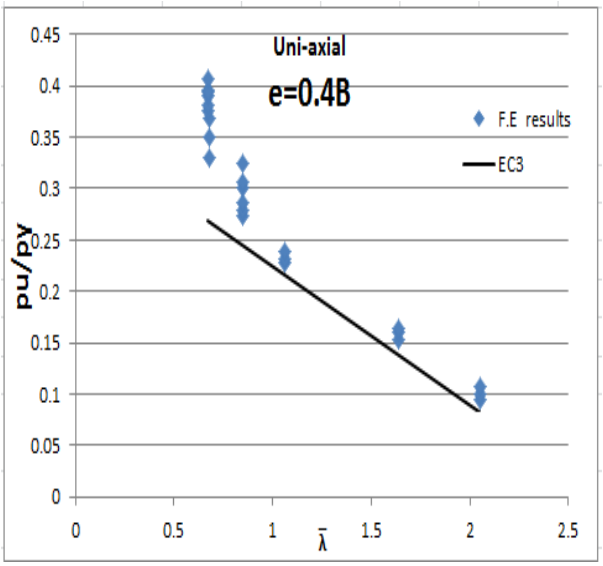


**Fig. 9. The ratio of (pu/py) the normalized axial forces to the non-dimensional slenderness for EC3[20] ($\bar{\lambda}$)**

## B. Failure modes' shape

For columns subjected to uni-axial loads, four primary failure modes occur due to buckling: local buckling, flexural buckling, distortional buckling, and lateral torsional buckling, which results from the buckling mode of shapes. Table 3 comprehensively summarizes the maximum load and the specific failure scenarios associated with each model.

In column model 2400B90-340U68, which had an ultimate load of 131.32KN, the waves of local buckling at the failure shape were seen to be more prominent at the column's web and flange and occur overall buckling of the section. However, for models 2400B40-340U20, 3000B60-250U30, 3000B40-250U48, B90A-340, and 2400B90-340U45, an interaction between flexural and distortional buckling was observed.

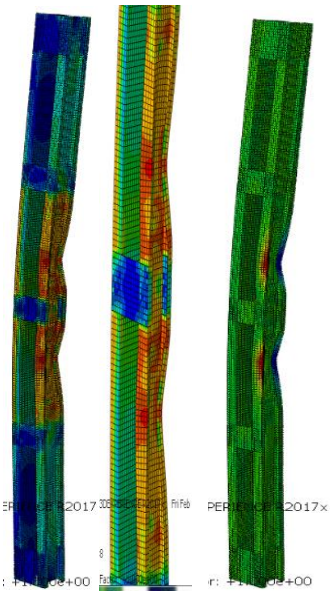

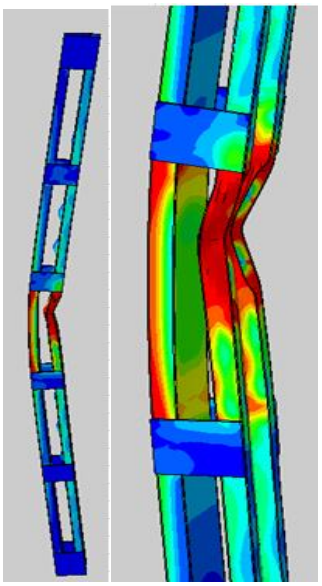

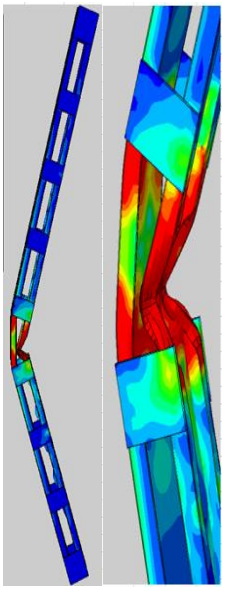

. 2400B90-

Journal of Engineering Research (JER)
ISSN: 2356-9441 Vol. 9 – No. 1, 2025 ©Tanta University, Faculty of Engineering e ISSN: 2735-4873

340U68 (F+L) 3000B60-460U56(F+L+D+LTB) 3000B60-250U30(F+L+D+LTB)

**Fig.10.The failure shape**

For column with slenderness ratios less than 1.1, failure is primarily dominated by local buckling, followed by distortional buckling modes. For higher slenderness ratios, failure is governed by a combination of distortional and flexural buckling modes.
The load-carrying capacity of built-up battened sections is largely influenced by the number of battens, as specified in design code provisions, and the spacing between the channels.

## D. Axial shortening versus axial load

The magnitude of the axial compression was measured at point 1, located at the loaded end of the column, as depicted in the finite element in Fig.2. Figure 11 describes the relationship between the uniaxial load and axial shortening of all cold-formed steel (CFS).

Figures 11 show the relationship between axial shortening and axial load response for columns with the same depth-to-width ratio (hw/B). As the overall slenderness ratio increases, the maximum strength of the columns decreases. The plots for uniaxial load versus axial shortening display only a slight nonlinearity before the columns reach their peak axial strength. After reaching peak behavior, the columns experience a gradual decrease in uniaxial strength. The failure mode of the columns is characterized by a combination of local and global (flexural) buckling, including lateral torsional buckling.

When the column depth-to-width ratio (hw/B) is ≤ 0.75 and the overall slenderness ratios are high, a significant nonlinear response is observed in the relationship between axial load and axial shortening.

For uniaxially loaded columns, when the eccentricity of the load (ex) is equal to 0.4B, the peak axial strength and axial shortening of the columns are influenced by the depth-to-width ratio (hw/B) for the same cross-section. For example, columns with a (hw/B) ratio of 0.7058 showed reductions in peak axial strengths of 14%, 9%, and 8% for slenderness ratios of λz = 450, 340, and 175, respectively, when the (hw/B) ratio increased from 0.7058 to 0.857. The reductions were 30%, 28%, and 25% when the (hw/B) ratio increased from 0.75 to 1.0 for λz = 450, 340, and 175, respectively.

Similarly, when the eccentricity of the load (ex) is equal to 0.5B, columns with (hw/B) of 0.7058 showed reductions in peak axial strengths of 2.5%, 1.9%, and 1.2% for λz = 450, 340, and 175, respectively, when the (hw/B) ratio increased from 0.7058 to 0.857. The reductions were 4.7%, 4%, and 5% when the (hw/B) ratio increased from 0.75 to 1.0 for λz = 450, 340, and 175, respectively.

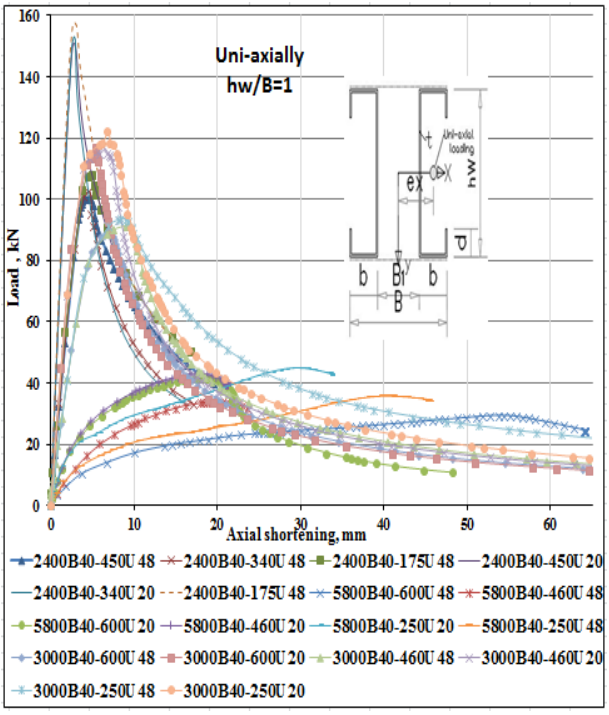


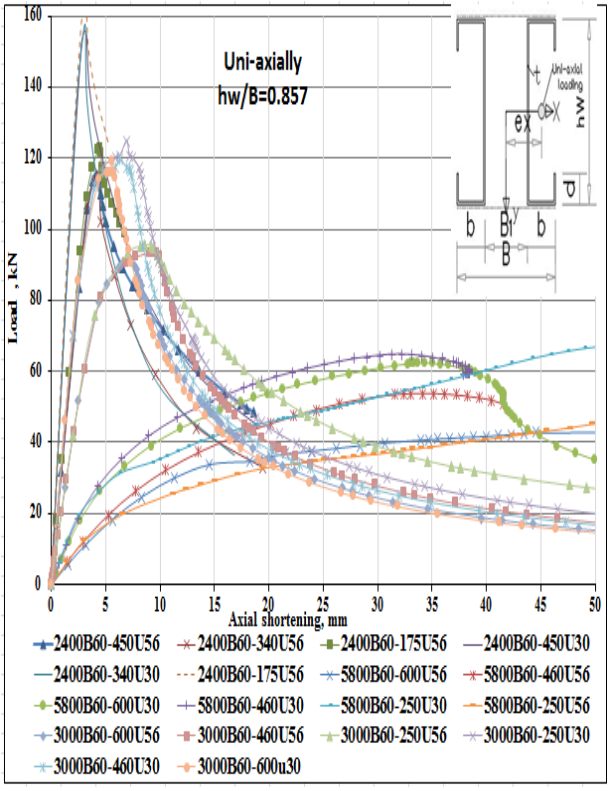




https://digitalcommons.aaru.edu.jo/erjeng/vol9/iss1/19
DOI: https://doi.org/10.70259/engJER.2025.911910

Journal of Engineering Research (JER)
ISSN: 2356-9441 Vol. 9 – No. 1, 2025 ©Tanta University, Faculty of Engineering e ISSN: 2735-4873

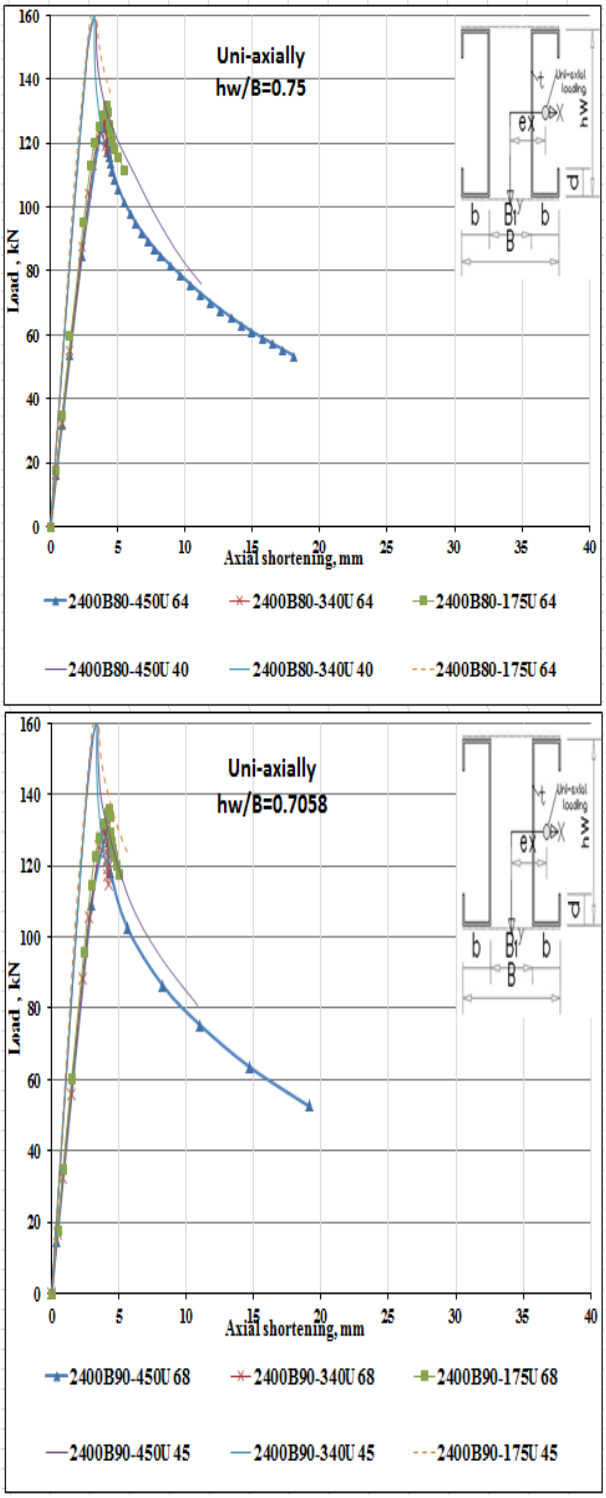


**Figure11: Relationships between load and axial shortening for uni-axially loaded columns**

## E. Load and lateral displacement (Ux and Uy)

Lateral displacements were measured at two points along the column: "point 2" at the midpoint of the column and "point 3" at the midpoint of the cross-sectional flange, as shown in Figure 2.

For a uniaxially loaded column, the lateral displacement in the x-direction (Ux) was more pronounced than in the y-direction (Uy). Figure 12 illustrates the relationship between the uniaxial load and lateral displacement response for columns with different channel slenderness ratios (λz). After short columns reach their peak strength, their strength drops significantly.

Columns with higher slenderness ratios exhibited better ductility compared to those with lower slenderness ratios. Thus, column ductility was directly related to the overall slenderness ratio. The lateral displacements (Δ) at which the columns reached their peak uniaxial strength were normalized by the column height (L).

The axial stiffness of a column under uniaxial loads was more evident for columns with a depth-to-width ratio (hw/B) of 0.7058 and 0.75. For columns with the same depth-to-width ratio, axial stiffness initially increased with the overall slenderness ratio. Additionally, columns with lower channel slenderness ratios (λz = 11.29) exhibited higher axial stiffness compared to those with slenderness ratios of 21.94 and 29.03.

Built-up columns made from unstiffened CFS channel sections were more prone to local buckling failures due to the absence of stiffeners in the chord members. As a result, the normalized lateral displacements of these columns showed a scattered upward trend. Furthermore, increasing the channel slenderness ratio (λz) resulted in higher lateral drift before failure and significantly reduced the scattering in lateral displacement.

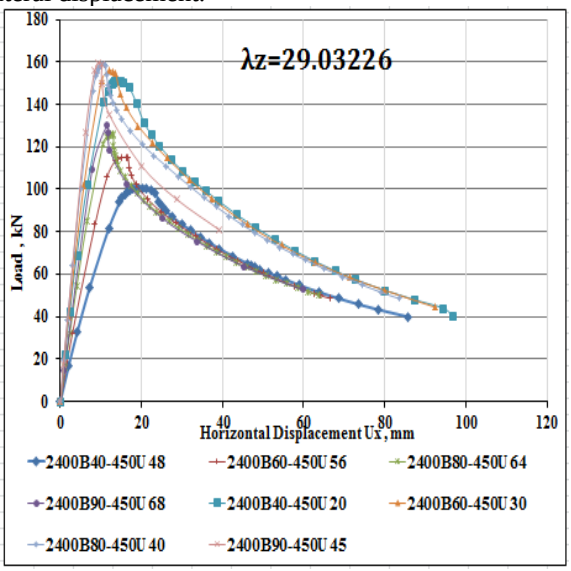

Journal of Engineering Research (JER)
ISSN: 2356-9441 Vol. 9 – No. 1, 2025 ©Tanta University, Faculty of Engineering e ISSN: 2735-4873

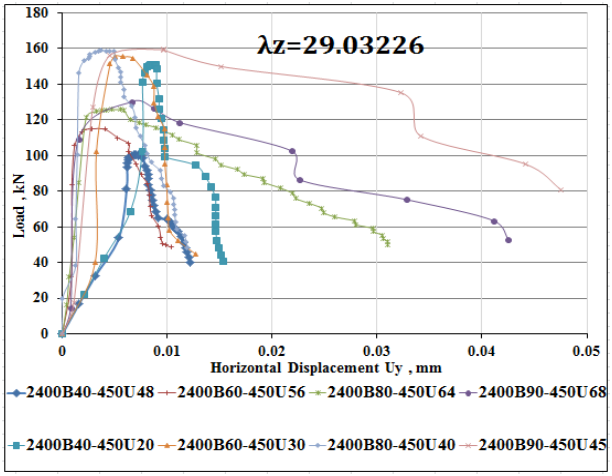


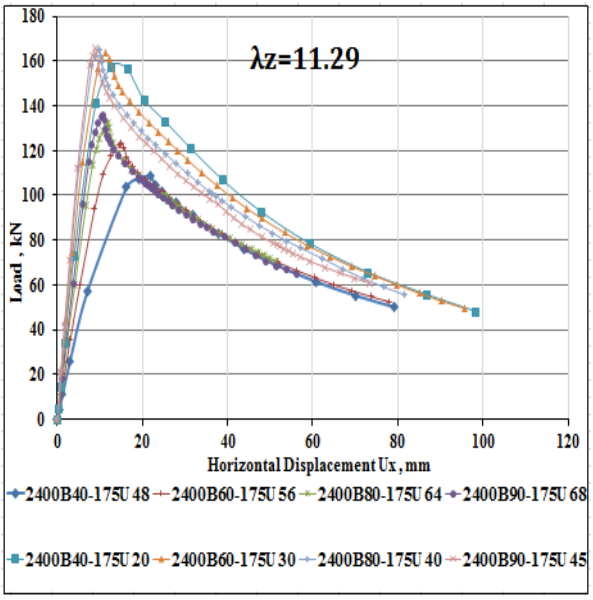


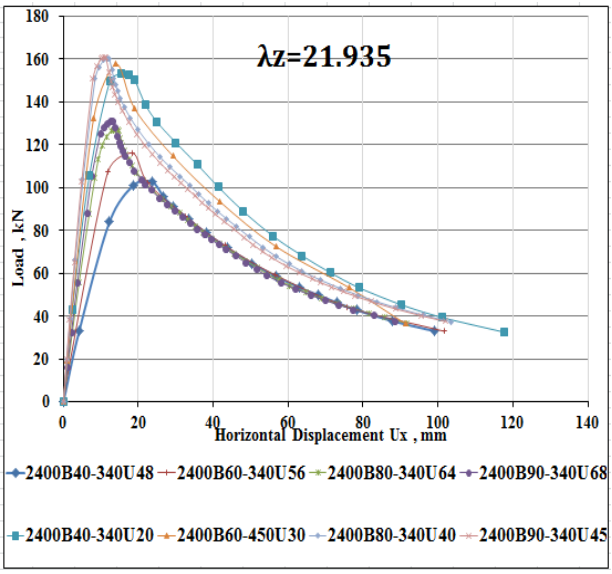


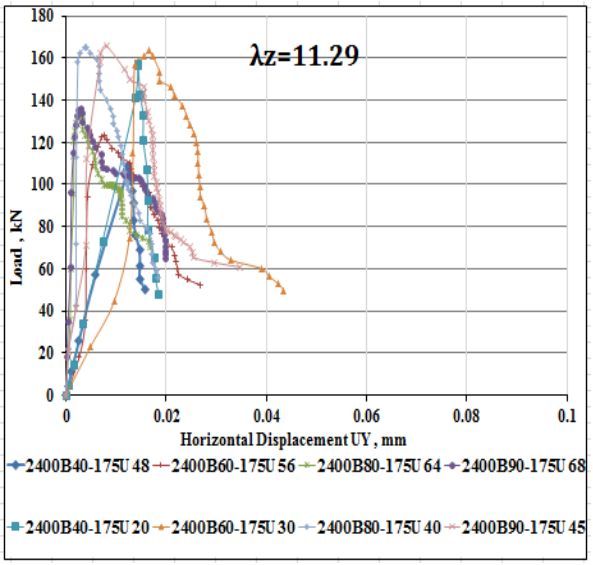


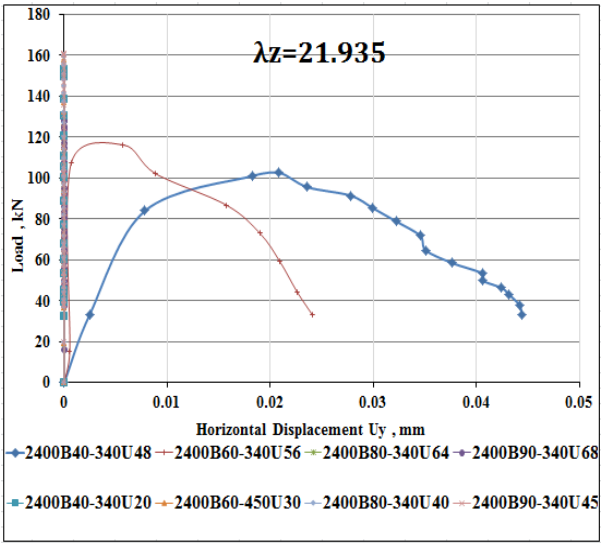


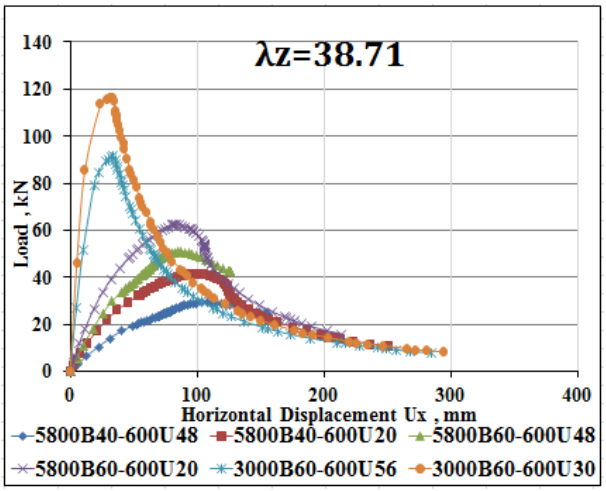




https://digitalcommons.aaru.edu.jo/erjeng/vol9/iss1/19
DOI: https://doi.org/10.70259/engJER.2025.911910

Journal of Engineering Research (JER)
ISSN: 2356-9441 Vol. 9 – No. 1, 2025 ©Tanta University, Faculty of Engineering e ISSN: 2735-4873

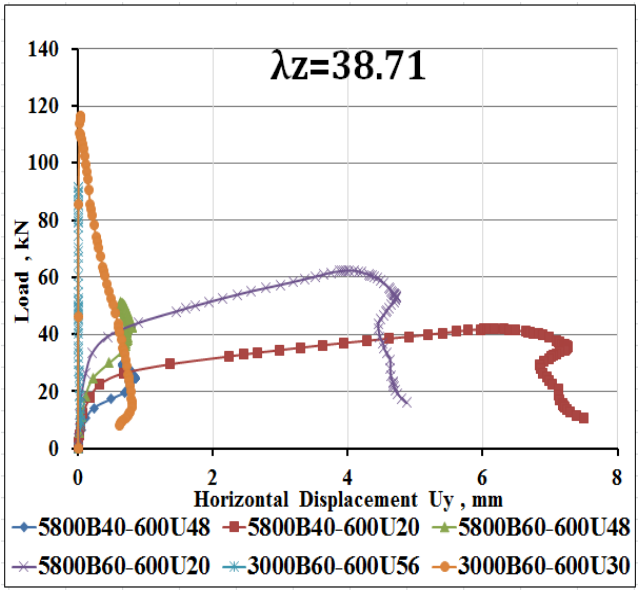


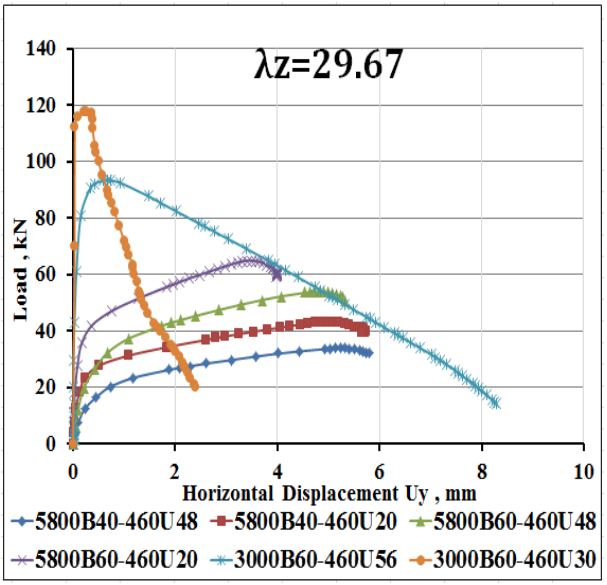


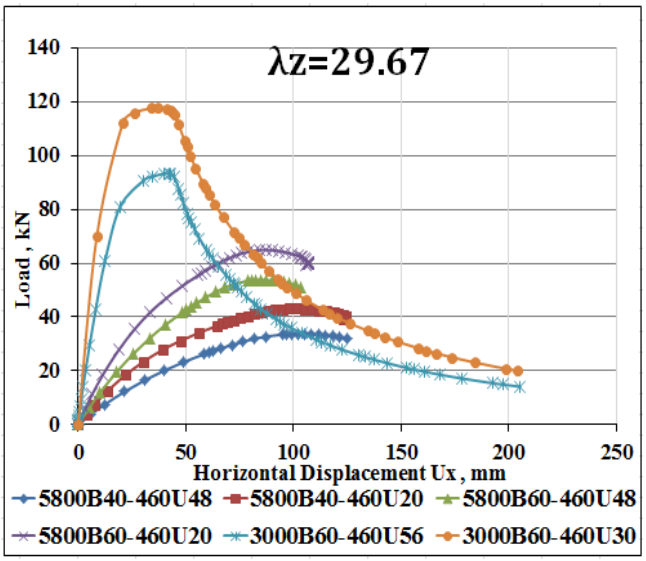


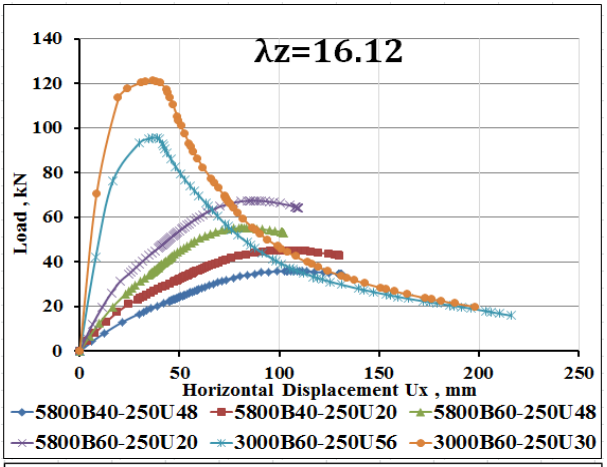


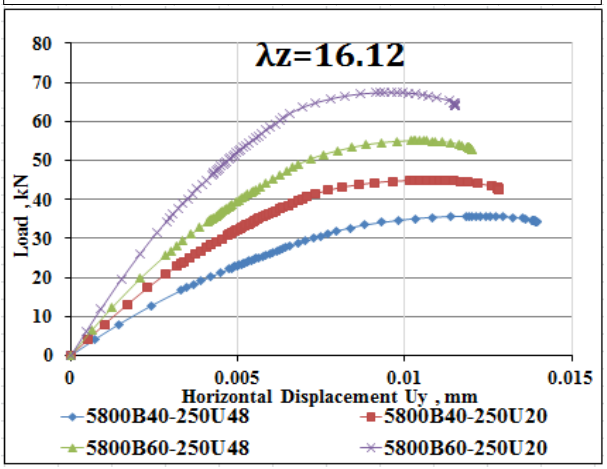


**Figure 12: Relationships between load-induced lateral displacements (Ux) and (Uy) for columns subj-ected to uniaxial loading.**

## VI. Conclusions

The study used a nonlinear finite element model to evaluate

Journal of Engineering Research (JER)
ISSN: 2356-9441 Vol. 9 – No. 1, 2025 ©Tanta University, Faculty of Engineering e ISSN: 2735-4873

the ultimate capacity of battened beam columns, composed of two cold-formed battened channel sections in a back-to-back arrangement. The model accounted for both geometrical and material nonlinearities. For uniaxially loaded columns, local buckling is the primary failure mode for short columns, while long columns fail due to flexural buckling, accompanied by local buckling. Intermediate columns fail due to a combination of local and flexural buckling (interactive buckling).

The Eurocode3 and AISI LRFD predictions for uniaxially loaded battened columns were found to be conservative, with Eurocode3 being less reliable than AISI. Initial geometrical imperfections ($\Delta = L/1000$) were included in all loading cases, even for axially loaded columns. Axially loaded columns showed the highest cross-sectional capacity, in contrast to uniaxially loaded columns, which exhibited significant flange buckling in the local channel for both short and medium columns.

The DSM approach's results were conservative for columns that fail due to local buckling, while they were slightly conservative for columns that fail due to global buckling. According to EC3 specifications, open sections are considered conservative for columns failing in local buckling and slightly conservative for those failing in global buckling. The interaction curves between axial load and moment take a concave downward shape for columns with intermediate slenderness ratios. Additionally, the study found that the ultimate strength is reduced by increasing the slenderness ratio of the channel between batten plates ($\lambda z$) or by decreasing the back-to-back distance between the channel sections.

**Conflicts of Interest:** The authors declare no conflict of interest.

## REFERENCES

[1] Blum HB, Rasmussen KJR, "Experimental investigation of long-span cold-formed steel double channel portal frames," J Construction Steel Res, vol. 155, pp. 316–330, 2019, DOI: https://doi.org/10.1016/j.jcsr.2018.11.020.

[2] Parastesh H, Hajirasouliha I, Taji H, Sabbagh AB, "Shape optimization of cold-formed steel beam-columns with practical and manufacturing constraints," J Construction Steel Res, vol. 155, pp. 249–259, 2019, DOI: https://doi.org/10.1016/j.jcsr.2018.12.031.

[3] Matsubara GY, Batista EM, Salles GC, " Lipped channel cold-formed steel columns under local distortional buckling mode interaction," Thin-Walled Structure , vol. 137, pp. 251–270, 2019, DOI: https://doi.org/10.1016/j.tws.2018.12.041.

[4] Lim JBP, Wrzesien AM, Nethercot DA, "Sustainable Applications of cold-formed steel structures: Portal frames Recent Trends in Cold-Formed Steel Construction," First Ed. Sawston, UK: Woodhead Publishing, pp. 265–303, 2016, DOI: https://doi.org/10.1016/B978-0-08-100160-8.00013-X.

[5] Dizdar C, Baran E, Topkaya C, "Strength and stiffness of floor trusses fabricated from cold-formed steel lipped channels," Eng. Structure, vol. 181, pp. 437–457, 2019, DOI: https://doi.org/10.1016/j.engstruct.2018.12.041.

[6] Chen M, Young B, "Structural behavior of cold-formed steel semi-oval hollow section beams," Eng. Structure , vol. 185, pp. 400–411, 2019, DOI: 10.1016/j.engstruct.2019.01.069.

[7] Eltobgy, HH., Abu-Sena, AB, Darwish, E., Nabil, A., "Experimental and Parametric Research on the Behavior of Cfs-Zee Section Under Cyclic Load", Journal of Al-Azhar Univ. Eng, Vol. 17(64):2022, 895 – 904, DOI: 10.21608/auej.2022.253802.

[8] Nabil, A., Abu-Sena, AB, Eltobgy, HH., Darwish, E., "The Behavior of the Cfs-Zee Section Under Monotonic Axial Load: An Experimental and Parametric Study", August 2022 Journal of Al-Azhar University Engineering Sector 17(64):867-880 DOI: 10.21608/auej.2022.253798

[9] Dar MA, Subramanian N, Dar AR, Majid M, Haseeb M, Tahoor M, " Structural efficiency of various strengthening schemes for cold-formed steel beams: Effect of global imperfections, "Steel Comp Structure, pp. 393–403, 2019, DOI: 10.12989/scs.2019.30.4.393.

[10] Roy K, Mohammad Jani C, Lim JBP, "Experimental and numerical investigation into the behavior of face-to-face built-up cold-formed steel channel sections under compression," Thin-Walled Structure, vol. 134, pp. 291–309, 2019, DOI: 10.1016/j.tws.2018.09.045.

[11] Roy K, Ting TCH, Lau HH, Lim JBP, "Experimental and numerical investigations on the axial capacity of cold-formed steel built-up box sections," J. Construction Steel Res. 2019; 160:411–27, DOI: https://doi.org/10.1016/j.jcsr.2019.05.038.

[12] Roy K, Ting TCH, Lau HH, Lim JBP, "Effect of thickness on the behavior of axially loaded back-to-back cold-formed steel built-up channel sections – Experimental and numerical investigation, "Structures. 2018; 16:327–46, DOI: https://doi.org/10.1016/j.istruc.2018.09.009.

[13] Roy K, Ting TCH, Lau HH, Lim JBP, " Nonlinear behavior of back-to-back gapped built-up cold-formed steel channel sections under compression," J. Construction Steel Res 2018; 147:257–76, DOI: https://doi.org/10.1016/j.jcsr.2018.04.007.

[14] Anbarasu M, Dar MA, "Axial capacity of CFS built-up columns comprising of lipped channels with spacers: Nonlinear response and design," Eng. Structure, vol. 213, pp.110559, 2020, DOI: https://doi.org/10.1016/j.engstruct.2020.110559

[15] Lorkowski P, Gosowski B, "Experimental and numerical research of the torsion problem of built-up steel columns laced in a single plane," Eng. Structure, vol. 160, pp.566-580, 2018, DOI: https://doi.org/10.1016/j.engstruct.2018.01.049.

[16] Dar MA, Sahoo DR, Jain AK, "Axial compression behavior of laced cold-formed steel built-up columns with unstiffened angle sections," J. Construction Steel Res. 2019; 162:105727, DOI: https://doi.org/10.1016/j.jcsr.2019.105727.

[17] Dar MA, Sahoo DR, Pulikkal S, Jain AK, "The behavior of laced built-up cold-formed steel columns: Experimental investigation and numerical validation," Thin-Walled Structure, vol. 132, pp. 398–409, 2018, DOI: https://doi.org/10.1016/j.tws.2018.09.012.

[18] Dar MA, Sahoo DR, Jain AK, "Compression capacity of short cold-formed steel built-up columns with double-lacing configuration and low sectional compactness,"Proc. SSRC Annual Stability Conf. St. Louse, Missouri, USA 2019;1:472–82.

[19] Dar MA, Pulikkal S, Sahoo DR, Jain AK, "Axial Resistance of Short Built-up Cold formed Steel Columns: Effect of Lacing Slenderness,"In: Prakash R, Dutta S, Inann, E, Dwivedy SK (Eds), Advanced Structure Vibration, Lecture Notes Mech. Eng. Springer. Singapore; 2020, DOI:10.1007/978-981-15-5862-7-2.

[20] EN 1993-1-3, Eurocode 3: Design of steel structures - Part 1-3: General rules - Supplementary rules for cold-formed members and sheeting, European Committee for Standardization, Brussels, 2006.

[21] AISI S-100, North American Specification for the Design of Cold-Formed Steel Structural Members, AISI Standard, Washington, DC, 2016.

[22] M.A. Dar, D.R. Sahoo, A.K. Jain, " Battened built-up cold-formed steel columns: strength and deformation behavior," in: S.B. Singh, D. Bhunia, G. Muthukumar (Eds.), Adv. Concr. Struct. Geotech. Eng., 2018, pp. 185–189. Bloomsbury.

[23] M.A. Dar, D.R. Sahoo, A.K. Jain, "Numerical study on the structural integrity of built-up cold-formed steel battened columns," in: R. Prakash, R. Suresh Kumar, A. Nagesha, G. Sasikala, A. Bhaduri (Eds.) Structural Integrity Assessment, Lecture Notes Mech. Eng., Springer. Singapore, 2020.

[24] M.A. Dar, D.R. Sahoo, A.K. Jain, "Axial Strength and Stability Behavior of Cold-Formed Steel Battened Closed Section Columns," SSRC Annual Stability Conf., Atlanta, Georgia, USA, 2020.

[25] M. Anbarasu, M.A. Dar, "Axial capacity of CFS built-up columns comprising of lipped channels with spacers: nonlinear response and design," Eng. Structure. 213 (2020) 110559, DOI: https://doi.org/10.1016/j.engstruct.2020.110559.



https://digitalcommons.aaru.edu.jo/erjeng/vol9/iss1/19
DOI: https://doi.org/10.70259/engJER.2025.911910

Journal of Engineering Research (JER)
ISSN: 2356-9441 Vol. 9 – No. 1, 2025 ©Tanta University, Faculty of Engineering e ISSN: 2735-4873

[26] ABAQUS Analysis User's Manual-Version 6.16, USA: ABAQUS Inc.,2016.
[27] M. Dabaon, E. Ellobody, K. Ramzy, "Experimental investigation of built-up cold-formed steel section battened columns," Thin-Walled Structures. 92 (2015) 137–145, DOI: https://doi.org/10.1016/j.tws.2015.03.001.
[28] El Aghoury MA, Salem AH, Hanna MT, Amoush EA, " Experimental investigation for the behavior of battened beam columns composed of four equal slender angles,"Thin Walled Structures 2010;48–9:669–83, DOI: https://doi.org/10.1016/j.tws.2010.03.007.
[29] Anbarasu M, "Behavior of cold-formed steel built-up battened columns composed of four lipped angles: tests and numerical validation," Advanced Structure Eng. 2020;23(1):51–64, DOI:10.1177/1369433219865696.
[30] Anbarasu M, Dar MA, "Improved design procedure for battened cold-formed steel built-up columns composed of lipped angles," J. Construction Steel Res , vol. 164, 105781, 2020, DOI: https://doi.org/10.1016/j.jcsr.2019.105781.
[31] ASCE. Minimum design loads for buildings and other structures, ASCE/SEI 7-05. American Society of Civil Engineers Standard; 2006.